공학박사학위논문

탄소/에폭시 수리를 위한
복합재 프린터

Composite Printer for Carbon/Epoxy Repair

2020 년 2 월

서울대학교 대학원

기계항공공학부

김 호 진

탄소/에폭시 수리를 위한 복합재 프린터

Composite Printer for Carbon/Epoxy Repair

지도교수 안 성 훈

이 논문을 공학박사 학위논문으로 제출함

2019 년 10 월

서울대학교 대학원
기계항공공학부
김 호 진

김호진의 공학박사 학위논문을 인준함

2019 년 12 월

위 원 장 : 김 종 원
부위원장 : 안 성 훈
위 원 : 차 석 원
위 원 : 이 윤 석
위 원 : 이 길 용 이길용

공학박사학위논문

탄소/에폭시 수리를 위한 복합재 프린터

Composite Printer for Carbon/Epoxy Repair

2020년 2월

서울대학교 대학원

기계항공공학부

김 호 진

Abstract

Composite Printer for Carbon/Epoxy Repair

Ho-Jin Kim
Department of Mechanical and Aerospace Engineering
The Graduate School
Seoul National University

Carbon-fiber composites are widely used in airplane, and the development of electric vehicles has spurred demand as interest in light materials has increased concurrently. Thus, researchers have begun to study how users of these products repair them, but the properties of fiber composites make it difficult to measure the level of destruction in repaired areas. The repair process is usually based on hand-lay-up. The success of this method depends on the repairer's proficiency, and it takes much labor and time to cut carbon fibers according to the size and shape of the repair part. Furthermore, the post-curing process also takes a long time, regardless of the size of the repair area. This can lead to a large amount of waste when repairing small components, such as the surfaces of car parts. Another issue is how best to evaluate the

repaired area. If monitoring the life cycle or deformation of the component is conducted, even after the repair has been carried it, the user can anticipate and prepare for repairs based on strain sensor data.

Studies of large equipment, such as conventional airplanes, and the use of automated tape layering (ATL) to make large carbon composite materials have been actively underway since 2016. However, most previous research has been aimed at producing large carbon-fiber composite materials and reducing the waste and labor required for repair processes. However, there are no automated processes for small-scale repairs. Various small devices, from vehicles to mobile phones, use composites and thus require appropriate repair processes. Studies focusing on these issues are still lacking. In this study, we developed a rapid curing carbon-fiber composite printer. This can achieve a uniform fiber composite by automating the fiber laying method. A rapid curing device using Joule heat is used for local repairs. The repair time is reduced by mounting the rapid curing device on the printer.

The proposed printing system is validated by comparing the recovery rates of undamaged specimens and double-lap repaired specimens. These repaired samples achieve uniform quality following repeated repair, and are thus superior to conventional hand-lay-up repaired samples. The use of the rapid curing system improved the recovery rate by 93% or more in the double lap test. As mentioned previously, the variables used to describe the repair performance, which may vary depending on the technician's proficiency, are stabilized under our

system. The rapid curing is also optimized by mounting a feedback system between the temperature and electric power. This achieves uniform recovery rates, regardless of user proficiency. Non-destructive testing is also possible if we attach highly sensitive nanoparticle sensors to the device. The quality of the repair is assessed based on the life cycle and deformation of adhesive repair patches, which are evaluated using the proposed sensors. In this study, we propose the use of a rapid curing carbon composite printer and nanoparticle sensors. We expect that the composite printer developed in our research can be used to support the development of carbon composite applications in industries such as electric vehicles and airplanes.

Keyword: Carbon fiber composite, Three-dimensional printer, Joule heat, Rapid curing, Structural health monitoring, Automated process

Student Number: 2014-21832

Table of Contents

List of figures

List of Tables

Chapter 1. Introduction

1.1 Overview

Recently, there has been an increased demand for composite materials such as carbon fiber-reinforced polymers (CFRPs), which are used in the manufacture of various structures such as wings of aircraft, cowl structures and connecting rods of vehicles. The demand for lightweight materials has increased in aircraft, automobile and mobile device industries. As the demand increases, various methods to repair cracked CFRP have been proposed. A repair method that uses bonded composite patches has been used widely among airplane industries in recent years [1-2]. Bonded patch repair is a mechanically efficient and cost-effective method for repairing composite structures. This technique can also be applied to automobile and mobile device industries and it offers many advantages over riveting and fastening, which can induce corrosion.

The present research is focused on bonded composite patch repairs, such as scarf and stepped joint repairs. Repairs using bonded composite patches are performed by adhesively bonding a patch to the damaged area. Some inherent drawbacks of this method are the long process time, the required chamber vacuum bags for curing [3], and the possibility of unintentional heating of the patched substrate. This method can have negative effects on other parts or repair processes, because if the substrate or other parts are heated, thermal expansion of the composite substrate and repair patches occurs. Therefore, it is best to avoid heat when the repair patch is being cured. Adhesives with low curing temperatures have been developed [4]. However, in field repair, a heating system is needed after bonding the repair patches. There are a number of methods for rapid curing via local heating. Microwave heating, induction heating, and Joule heating could be used as an alternative post-heating process [9, 10]. The microwave heating and induction heating systems require a large-volume structure. Rapid curing via Joule heating can reduce composite patch repair processing times sharply, but studies about the Joule heating method for curing CFRP are limited.

A Joule heating system that can heat locally and rapidly is developed in this research. This method allows for greater control over the distribution of heat, which is applied only to the composite patch and can reduce the curing time. Carbon fiber can be used as a heating element in the rapid curing of adherents and adhesives. Bonded patch repair brings many advantages over mechanical fastening or riveting, including improved mechanical property behavior, restored stiffness and strength, minimal changes to the shape of the original structure, reduced weight, reduced corrosion and reduced cost of repair.

The Joule heating method is effective for individual repairs by members of the general public, but it is not ideal for commercial repairs because the procedure is usually done manually, and the quality of the repair typically depends on the technician’s skill [5-8]. Therefore, this research proposes and fabricates an automated direct carbon-fiber composite patch-printing system.

After composite patch repair, structural health monitoring (SHM) is used to gather data for aerospace and civil and mechanical engineering industries [11]. With the development of sensor technologies, monitoring algorithms, and system maintenance models [12-14], SHM has become an efficient engineering tool, reducing repair costs and the downtime of structures or systems. Recent advances in inkjet printing techniques have shown promise for sensor printing [17, 18]. However, there are some manufacturing problems; therefore, in this research, the proposed sensor is printed via another manufacturing process.

An essential part of SHM is the collection of various physical quantities of the appropriate sensors, such as displacement, forces, vibrations and acoustic emissions [15]. With respect to the designed purpose or function of the system, single or multiple types of sensor signals are collected and analyzed for the operation diagnosis. Mechanical strain is the most commonly used measurable sensor signal, because it is easy to implement and represents the system’s health status well, delivering physical information including the damage locations [16].

In this study, a directly printed strain sensor is proposed with solvent-free silver nanoparticles for the SHM of the CFRP. The strain sensor is printed onto the composite repair patch and its performance is evaluated in terms of the gauge factor, measurable strain range. An aerodynamically focused nanoparticle (AFN) printer is utilized to print the strain gauge patterns onto the CFRP [23]. AFN printing is a solvent-free, room temperature, direct printing dry technique. The process parameters of the AFN printer (the excitation valve timing and the stage speed) are studied and optimized to achieve high resolution (on the order of tens of nanometers) conductive patterns. With the optimized printing conditions, successful strain sensors are printed onto the various types of composite substrates, including the CFRP repair patches. The characteristics of the printed sensors are evaluated and compared to a commercial strain gauge using bending tests. The designed and printed sensors can be used not only for repair process monitoring but also for SHM as well as for non-destructive evaluation (NDE) purposes of the repaired composites [24, 25]. This research evaluates the composite repair process using this rapid curing carbon-fiber composite printing system and a highly sensitive sensor patch with a communication system.

1.2 Carbon fiber reinforced plastic (CFRP)

Carbon fiber-reinforced plastic (CFRP) is a composite material. A composite material consists of different two or more constituent materials with significant physical or chemical properties. When the two materials are combined as a composite material, the properties change. CFRP is strong and lightweight and has good iso- and anisotropic properties. Such properties have merits for the airplane and automobile industries.

1.3 CFRP repair

The more CFRP is used, the more damage may occur [26]. But the repair of CFRP poses a number of challenges [21, 27]. Damage can vary in size and depth. If every layer of the part is damaged, the whole structure must be replaced. However, surface cracks or scratches can be repaired by filling the layers. Bonded patch repair can be used in this case. This research is focused on bonded composite patch repairs, such as scarf and stepped joint repairs. Repairs using bonded composite patches are applied by adhesively bonding a patch to the damaged area. Bonded joint repair employs soft-patch adhesion using a wet lay-up or prepreg stacking and a hard-patch technique, in which a new patch is bonded using an adhesive. Normally, repair proceeds by hand, because crack depths and ranges vary greatly. Hand lay-up is difficult and much more time-consuming than automated CFRP fabrication [28]. Automated

Tape Laying (ATL) is one of the most well-established automated manufacturing techniques for composites. ATL typically uses wide unidirectional tapes that are placed onto a part mold using a loaded roller system with varying degrees of articulation, depending on the complexity of the part. ATL essentially replicates the manual deposition of uni-direction (UD) tape, but at higher speeds, on larger parts, and with greater process control. Although not necessarily a fiber placement technique, modern ATL systems have precise control of the tape start, cut, and orientation, allowing more complex reinforcement.

Part size and design are key drivers for composite tape layer efficiency. As a rule of thumb, bigger parts and simpler lay-ups are more efficient. If the design is highly sculptured (lots of ply drop-offs) or the part size is small, the machine will spend a significant amount of time slowing down, cutting and then accelerating back to full speed. Another limitation of ATL is the requirement of an additional manufacturing process for curing. In the repair process, the curing process is the most time-consuming procedure, regardless of the fabrication size.

1.4 The goal of this research

The goal of this dissertation was to develop a composite printer for carbon/epoxy repair with rapid curing. Moreover, to evaluate the performance of the developed printer system, a wireless data communication system that measures the strain and quality of printed repair patches via in-situ sensing is proposed.

To create this system, an automated carbon fiber laying system with an epoxy feeding control system and Joule heating module for curing is developed. An in-situ sensor patch with a wireless communication system is also proposed using an AFN printer.

First, various parameter tests were conducted for the design and fabrication of an automated carbon fiber printing system. Second, to evaluate the quality of printing, printer-repaired CFRP samples were fabricated for comparison with hand-repaired CFRP samples. Finally, structural health monitoring (SHM) data of printed repair patches were measured and transferred using highly sensitive strain sensor patches printed via the AFN printer with the communication system.

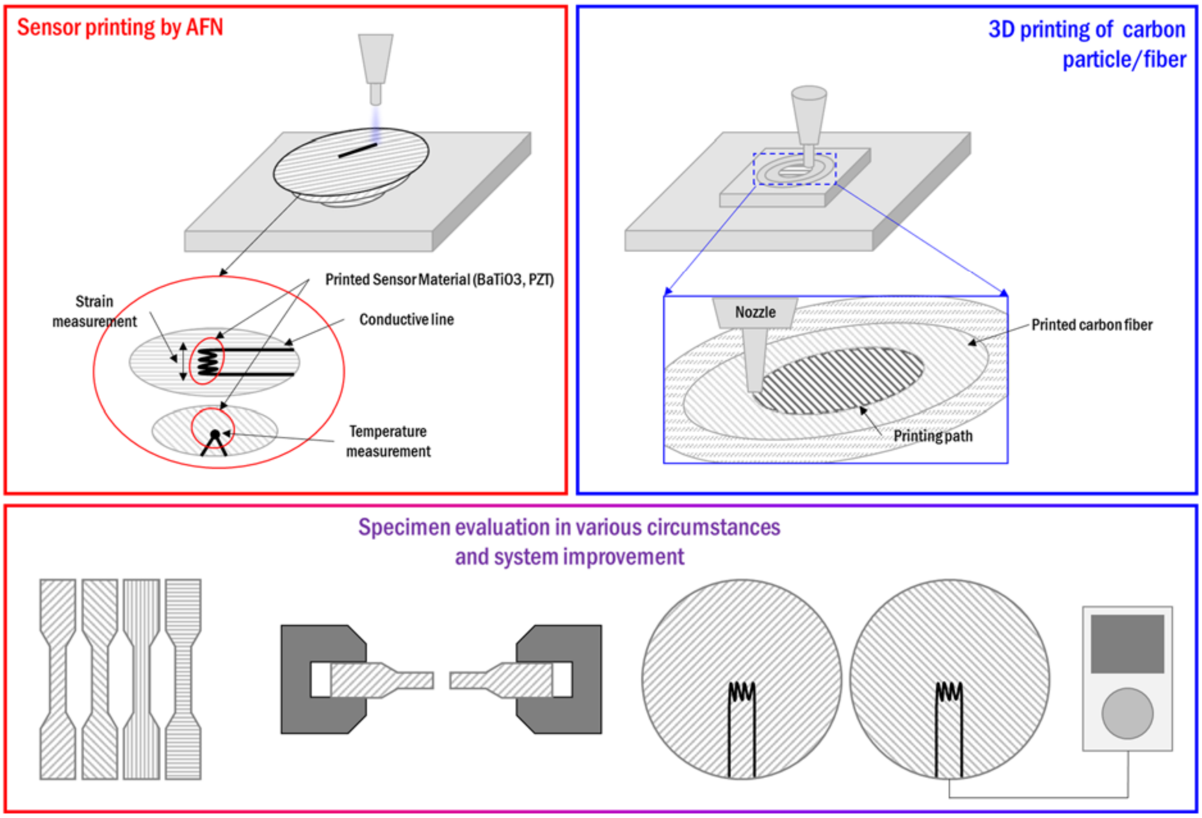

Figure 1 Overview of research

1.5 Outline of dissertation

Chapter 2 presents the background of CFRP industries, repair processes and SHM with the latest development. The main reason for the CFRP industry growth is introduced and detail repair types and methods are introduced in this chapter. In addition, the SHM for composite materials is introduced.

Chapter 3 introduces actual factors for the fabrication of automated fiber laying system and dimension decisions and a rapid curing system. The heating model of the rapid curing system is also proposed and using this model, the parameter for the proposed design is determined. The purpose of the fabricated components is presented such as the mechanism and the relationship between fiber-epoxy feeding and curing parameters, and a highly sensitive sensor with the communication system is also introduced.

Chapter 4 focuses on evaluations of developed devices. In the first, the printed sample of standard deviation between repeatable sample fabrication and recovery rate of the developed printing system. Also, the rapid curing system which can reduce whole repair process time is evaluated. The degree of cure is measured based on the conventional test method using the dialectical sensor. Finally, the resolution of the sensor patch is compared with commercial strain gauge and also evaluated wireless data transfer rate.

The contribution and originality of this research are summarized in chapter 5, together with the appendix and suggestions of future prospects to conclude this dissertation.

Chapter 2. Background

2.1 Demand for CFRP

A number of industries require lightweight materials and product designs, particularly aviation industries, where key elements of products include large rotating parts (e.g., the rotor blades of wind turbines), and the automotive industry, where driving dynamics are a major consideration. Global trends towards CO2 reduction and resource efficiency have significantly increased the importance of this topic over the last few years.

Overall, the use of lightweight materials in various industries, such as automotive, aviation, and wind, will increase significantly over the next two decades, leading to a market of more than USD 300 billion for high-strength steel, aluminum, and carbon fiber. Traditional steel will be substituted to a large extent by high-strength steel, and the highest growth will occur for carbon fiber, at almost 20 percent per year.

Recent prominent examples support the observation that this trend is gaining momentum: the Boeing 787 Dreamliner is constructed with over fifty-percent carbon-fiber-reinforced plastics (carbon fiber in the following) instead of having a traditional aluminum body structure. The use of carbon fiber bearings for an Airbus A340 horizontal tail reduces its weight by 50 percent and cost by 30 percent. The use of carbon fiber in the aviation industry is expected to grow further in the coming decades. The importance of lightweight materials will also increase significantly in the automotive industry, and the share of lightweight materials used in production is projected to more than double in the next 20 years.

2.2 Bonded patch repair

There are various types of composite repair methods, such as cosmetic, resin injection, structural mechanically fastened patches, structurally bonded patches, and scarf joints [29]. Of course, the repair method used depends on the size and depth of the cracks, but the specification and oversight of repair procedures can make it difficult to detect dangerous levels of structural fatigue, especially when such fatigue is a direct or indirect consequence of a repair. The well-known mechanism by which fatigue propagates through a structure is that of the crack. Cracks propagate because of their geometry. Something produces a high stress-concentration at the end of the crack. If a growing crack is not tracked, the material will fracture. Fatigue cracks have been found to arise in several ways, particularly from fastener holes such as those for rivets, bolts, nuts, and screws, where localized stress can initiate premature cracking. Stress can also become concentrated during repairing processes, and this should also be avoided. There are some disadvantages to repairing these types of cracks: stress concentrations at fastener holes, difficulties in detecting cracks under patches, rapid crack growth at the end of the repair patch, danger of corrosion under the patch, etc. In this respect, composite patch bonding repair has many advantages: no damage to the structure or hidden components, slow crack growth even at the bond line between the patch and the substrate, high repair quality, ability to detect crack growth under the patch, no corrosion problems, sealed interface, etc.

Patch bonding repair methods can be divided into three types. First, the hard-patch method, in which a new patch is bonded using an adhesive. The second method involves a soft-patch adhesion, using a wet lay-up or prepreg stacking. The other type involves lap-joint bonding, in which a single external doubler is often used to repair lightly loaded thin laminate structures [30, 31].

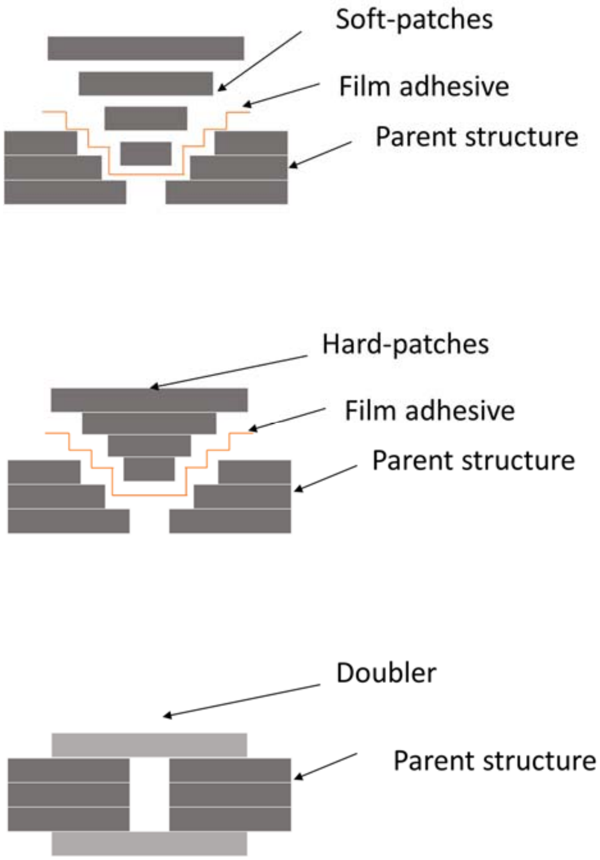

Figure 2 Bonding patch repair types

Especially, the geometry of a double-lap joint is shown in Figure 2. The free-body-diagram of interfaces-force in the overlap region is shown in Figure 3. The equilibrium of upper and lower adherend is achieved to the following differential [32]:

$$\frac{dT_0}{dx} + \tau = 0 \tag{2-1}$$

$$\frac{dT_i}{dx} - 2\tau = 0 \tag{2-2}$$

where T_0, T_i in equations (2-1) and (2-2) shows longitudinal tension per unit width of the upper and lower adherend, each, τ is the shear stress in the adhesive layer. The longitudinal displacement and strain relation of adherends are:

$$\frac{du_0}{dx} = \varepsilon_0 = \frac{T_0}{E_0 t_0} \tag{2-3}$$

$$\frac{du_i}{dx} = \varepsilon_i = \frac{T_i}{E_i t_i} \tag{2-4}$$

The longitudinal displacement, strain, Young's modulus and thickness of the outer adherend is claimed as u_0, ε_0, E_0 and t_0, respectively. u_i, ε_i, E_i and t_i are the respective values relative to the inner adherend. The differential equation (2-3) and (2-4) can be applied together through the shear deformation in the adhesive layer as follows:

$$\tau = G_a\gamma = \frac{G_a}{\eta}(u_i - u_0) \quad (2\text{-}5)$$

and thickness of the adhesive layer, respectively. Taking the derivative with respect to x of equation (2-5) and equation (2-1), derives

$$\frac{d\tau}{dx} = \frac{G_a}{\eta}\left(\frac{du_i}{dx} - \frac{du_0}{dx}\right) \quad (2\text{-}6)$$

$$\frac{d^2T_0}{dx^2} = -\frac{d\tau}{dx} \quad (2\text{-}7)$$

Substituting equation (2-6) and equation (2-3) and (2-4) into equation (2-7) yields

$$\frac{d^2T_0}{dx^2} = -\frac{G_a}{\eta}\left(\frac{du_i}{dx} - \frac{du_0}{dx}\right) = -\frac{G_a}{\eta}\left(\frac{T_i}{E_iT_i} - \frac{T_0}{E_0T_0}\right) \quad (2\text{-}8)$$

The equilibrium of force requires that the sum of longitudinal forces in outer and inner adherend equals to the applied force P, such as

$$P = T_i + 2T_0 \quad (2\text{-}9)$$

Substituting equation (2-9) into (2-8), one can obtain a second-order differential equation of T_0 with respect to x as follows:

$$\frac{d^2T_0}{dx^2} = -\lambda^2 T_0 = -\frac{G_a P}{E_i t_i \eta} \tag{2-10}$$

where

$$\lambda^2 T_0 = \frac{G_a}{\eta}\left[\frac{2}{E_i T_i} - \frac{1}{E_0 T_0}\right] \tag{2-11}$$

and the boundary conditions are

$$T_0 = 0\,,\ x = \frac{l}{2}$$

$$T_0 = -\frac{P}{2}\,,\ x = -\frac{l}{2} \tag{2-12}$$

where λ is the length of the bonded region.

The solution of differential equation (2-10) can be written as

$$T_0 = A\,sinh(\lambda x) + B\,cosh(\lambda x) + \frac{PE_0 t_0}{(E_i t_i + 2E_0 t_0)} \tag{2-13}$$

To apply the boundary condition in equation (2-12), the integration constants A and B can be solved. As a result, the longitudinal tensions,

T_0 and *T_i*, between adherend layers and the shear stress in the adhesive layer can be expressed as the following forms:

$$T_0 = \frac{P}{2}\left[-\frac{1}{2}\frac{sinh(\lambda x)}{2sinh\left(\frac{\lambda l}{2}\right)} + \frac{E_i t_i - 2E_0 t_0}{2(E_i t_i + 2E_0 t_0\ )}\frac{cosh(\lambda x)}{cosh\left(\frac{\lambda l}{2}\right)} + \frac{2E_0 t_0}{(E_i t_i + 2E_0 t_0)}\right] \qquad (2\text{-}14)$$

$$T_i = P\left[1 + \frac{1}{2}\frac{sinh(\lambda x)}{2sinh\left(\frac{\lambda l}{2}\right)} - \frac{E_i t_i - 2E_0 t_0}{2(E_i t_i + 2E_0 t_0\ )}\frac{cosh(\lambda x)}{cosh\left(\frac{\lambda l}{2}\right)} - \frac{2E_0 t_0}{(E_i t_i + 2E_0 t_0)}\right] \qquad (2\text{-}15)$$

$$\tau = \frac{P\lambda}{4}\left[\frac{cosh(\lambda x)}{sinh\left(\frac{\lambda l}{2}\right)} - \frac{E_i t_i - 2E_0 t_0}{2(E_i t_i + 2E_0 t_0\ )}\frac{sinh(\lambda x)}{cosh\left(\frac{\lambda x}{2}\right)}\right] \qquad (2\text{-}16)$$

The constants E_i and E_0 are the equivalent longitudinal modulus in inner and outer adherends, respectively [32, 33]

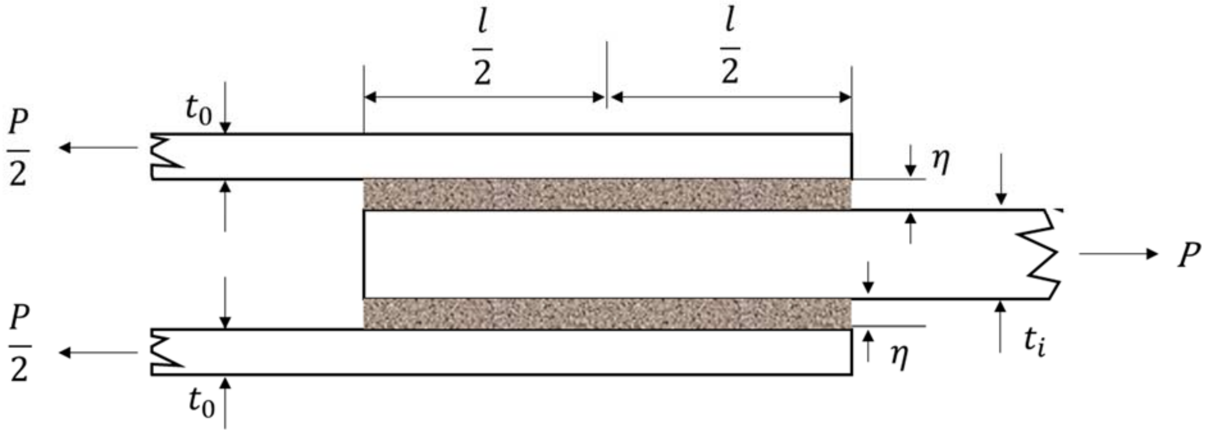

Figure 3 Geometry of schematic of a double lap joint [1]

2.3 Structural health monitoring (SHM)

Recently, the importance of SHM has raised for the aerospace, civil and mechanical engineering infrastructures [4]. The history of SHM could be introduced for understanding the development of SHM technology [39]. The current study has begun to recognize that the SHM problem is basically one of the statistical pattern recognition (SPR) and a paradigm to address such a problem is described in detail as it forms the fundamental for the organization of this theme issue. In conclusion, technical challenges that will be addressed if SHM is to gain wider applications are discussed in a general manner.

Most recent structural and mechanical system maintenance is conducted in a time-based. As an example, Recently, Airbus presents the law of 'SHM of Airbus A380', which is missiles are retired after a set number of captive-carry hours on the wing of an aircraft [40-42]. SHM is the technology that will allow the current time-based maintenance philosophies to evolve into potentially more cost-effective condition-based maintenance philosophies. The concept of condition-based maintenance is that a sensing system on the structure will monitor the system response and notify the operator that damage has been detected. When the monitoring system provides sufficient warning such that corrective action can be taken before the damage evolves to a failure level, economic benefits, and safety for life associated with such a philosophy will only be realized [43-46]. The trade-off associated with implementing such a philosophy is that it requires more sophisticated monitoring hardware to be deployed on the system and it requires a sophisticated data analysis procedure that can be used to interrogate the measured data.

This research is focused on the composite strain or delamination of structure. The concept of structural health monitoring is particularly important for fiber-reinforced composites due to the complexity of the possible failure mechanisms. The industry also needs SHM for the same reason for this research purpose. First, almost every industry, which applies SHM, wants to detect damage in its structural and mechanical infrastructure at the earliest possible time. Industries' desire to perform such monitoring is based on the tremendous economic and life-safety benefits and this technology has the potential to offer.

Chapter 3. Design and fabrication

3.1 Direct carbon printing system

3.1.1 Overview of printing system

Figure 4 shows the traditional carbon fiber composite repair process. In step 1 in the figure, the crack depth and the dimensions of the area to be removed are determined, normally via non-destructive infrared thermography (IRT) that does not affect the surrounding area. IRT yields data on the impact that caused the damage, the resulting fatigue, and delamination [47-51]. Fiber-reinforced plastics usually are fabricated using lamination so, sometimes the damaged area is not detected when seeing the outfit of structures. That is why the non-destructive inspection method uses in damage detection in CFRP industries. After inspection and determine the scale of repair area, cracked area is cut off using conventional milling and grinding. Typically using a hand tool; the efficacy of FRP machining is critically dependent on the tools employed and their skill [4, 52, 53]. The cut area is usually stepped at a defined taper angle chosen by reference to the shape and the joining method employed. Bond repair patch types such as scarf joints are commonly created; these distribute stress effectively to the borders of structures. The CFRP structure is laminated, the diameter of the cut area varies by layer, increasing in a step-like manner. These procedures of repair are also studied by various research groups. The repair patches are fabricated in step 3; their dimensions are those of the slots created in step 2. As a modulus loss (compared to that of non-repaired CFRP) is inevitable, it is usual to add a few additional layers to the surface of the repaired structure. Hard patch repair minimizes inter-layer deformation [4]. However, pre-cured patches must be initially molded. Of the soft patch techniques, the prepreg is costly in terms of both storage and transport [54-56]. After this process, there is time-consuming process for fabricating repair patch. Proposed rapid curing carbon fiber composite printing system in this research targets on steps three and four in Figure 4. After cutting off the area, a composite repair patch has to fill out through properly sized patches [57]. In this process, repair quality could be changed according to the skill of a technician. It means the life of the repair patch is not guaranteed [58]. In this research, the carbon fiber printer is developed for these ends. Continuous carbon fibers overlaid with epoxy resin are produced, and the print length is controllable. The proposed printer makes repair parameter standardized, which means regardless of the skill of the worker the quality of repair is normalized. The last step of the repair is the post-curing process. Normally, this process takes a long time of whole repair time. This printer involves the rapid curing system for reducing this curing time. The detail mechanism and configuration of components are explained next.

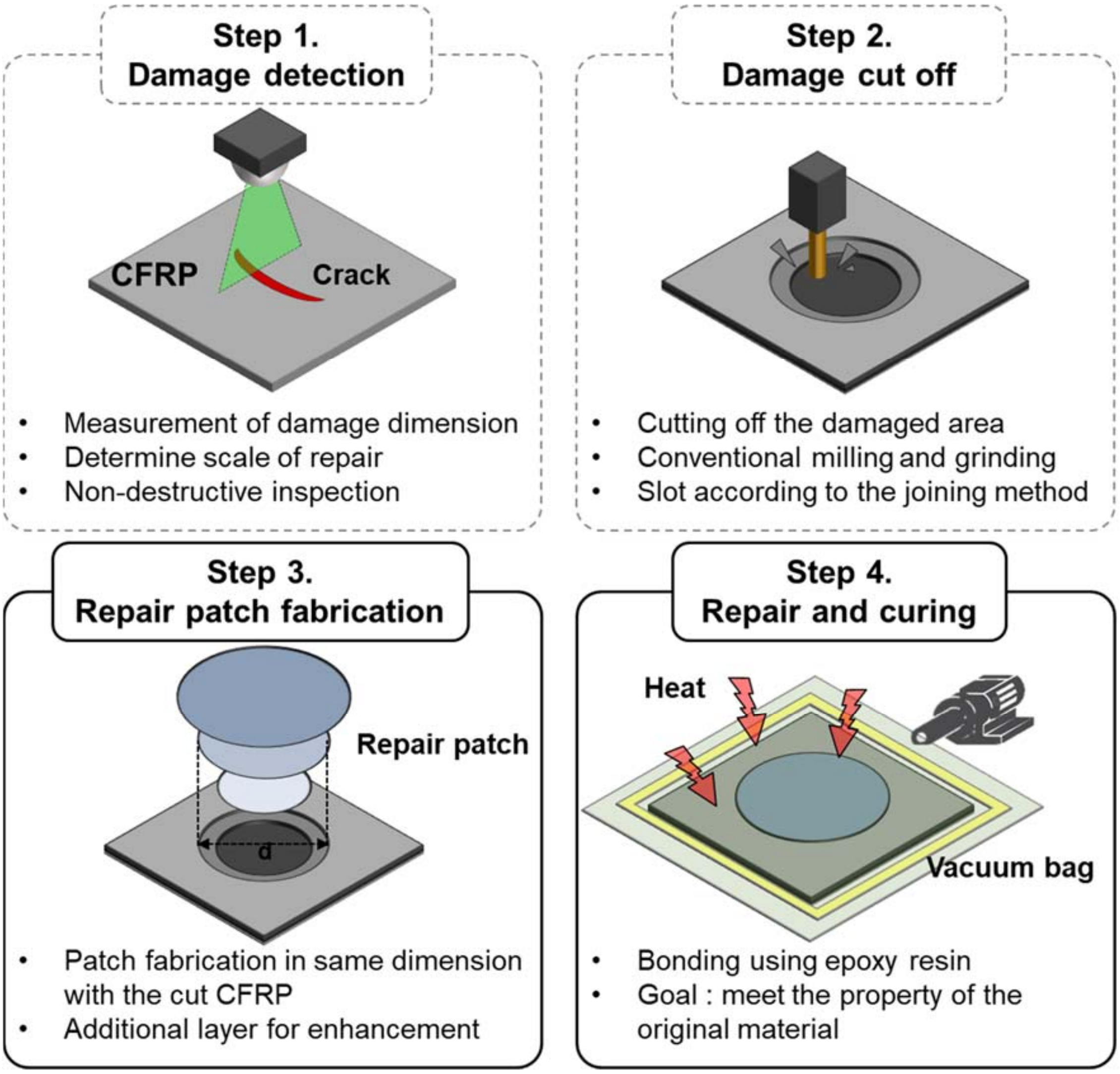

Figure 4 Conventional repair process

Figure 5 shows the four-axis rapid curing carbon fiber composite printing system. The system contains the direct fiber printing head, epoxy feeding system and rapid curing system with the gantry type. The motion stage consists of X-axis and Y-axis on the floor and Z-axis and R-axis on the gantry.

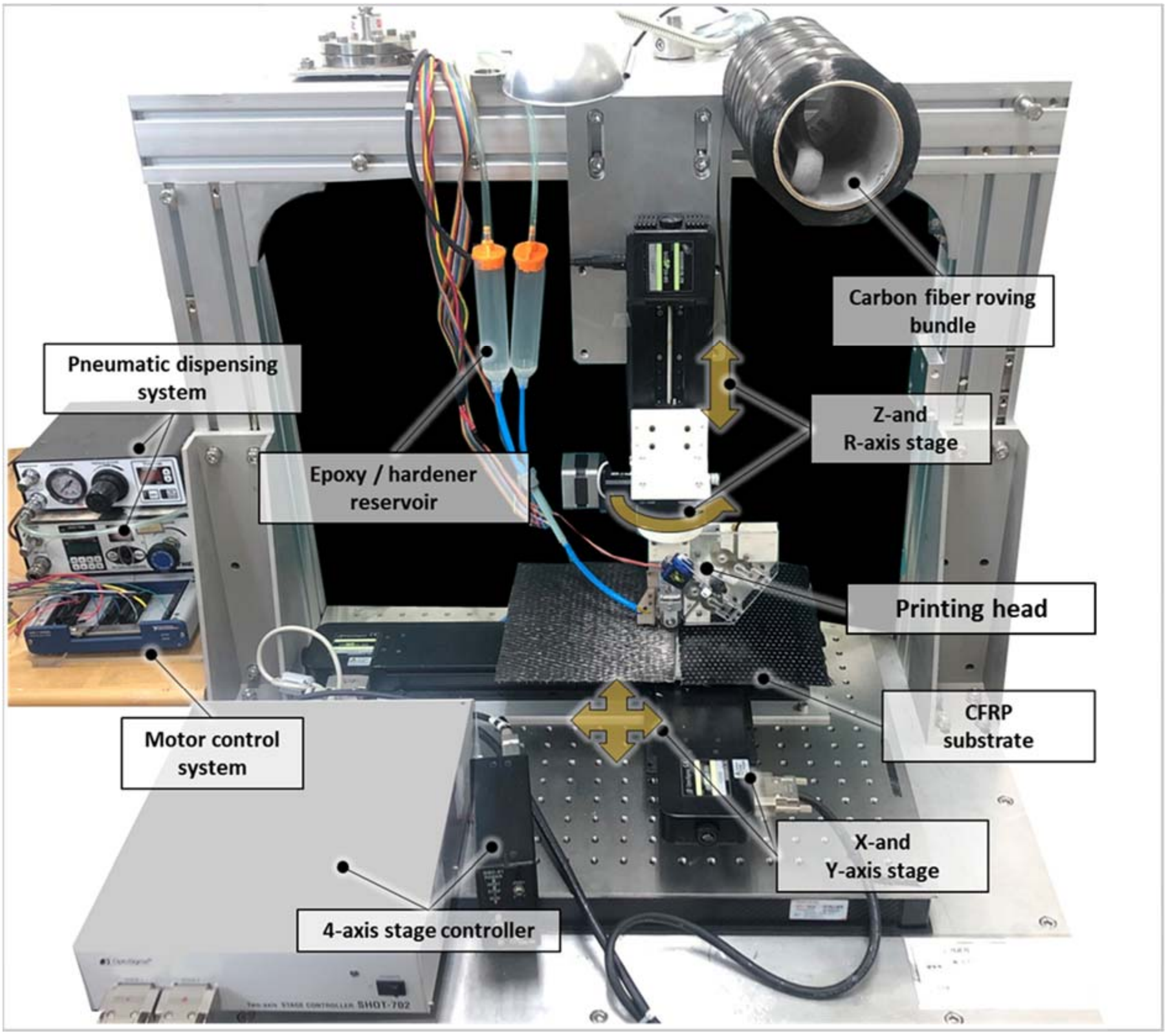

Figure 5 Carbon composite printer

The stroke of the motion stage for the XY-axis is 850 mm and a prototype of the proposed printing head. Although travel is not enough for making some part of the airplane. However, this research target of printing is a repair patch so it is enough to fabricate repair samples. There are the controllers for stages, dispensing controller for epoxy feeding, printing head with fiber feeding control module and rapid curing module in front of the printing head. The detailed mechanism and design parameters are explained following chapters.

3.1.2 Fiber feeding component

Figure 6 shows the printer head schematic diagram; this features a fiber-feeding system, fiber-cutting, and fiber-layering. The red path is that of a dry fiber through the feeding and cutting modules; layered fibers are then placed on the substrate. The epoxy resin is applied to the dry fiber during its travel, thus, before the fiber attains the cutting module then cutting during travel controls the length of the printed fiber.

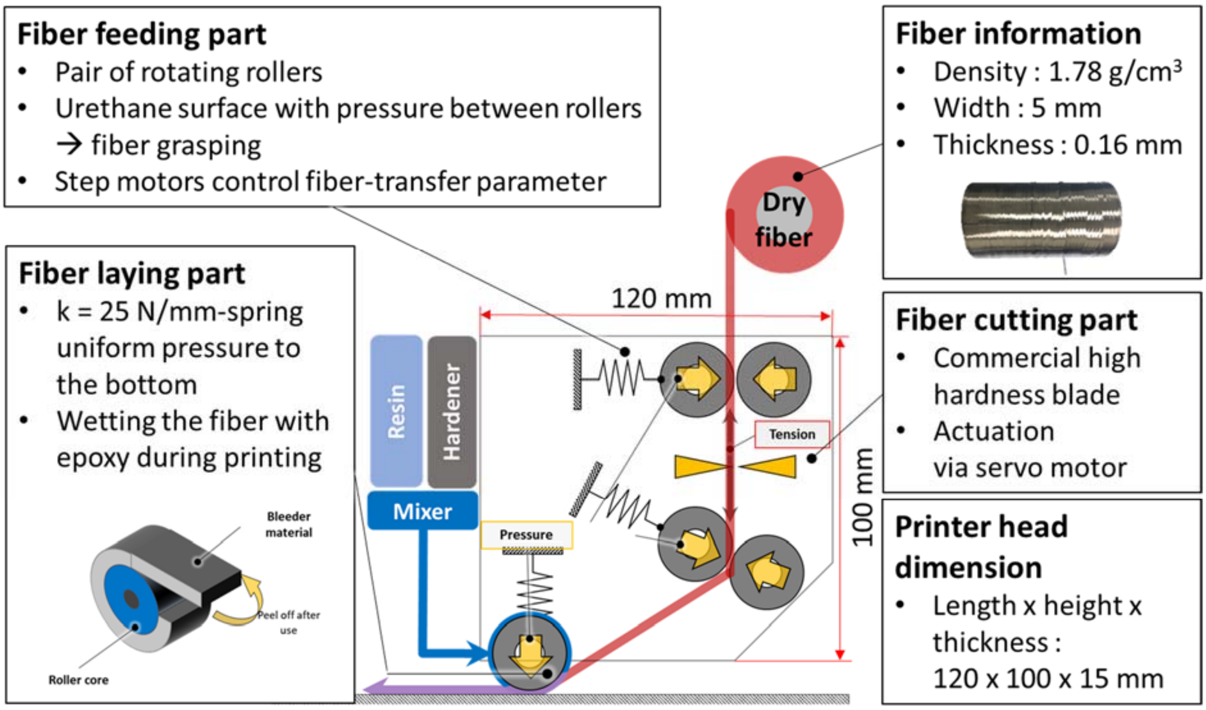

Figure 6 A schematic of printer head

Fiber-feeding is performed using two identical urethane-covered rollers that firmly grasp the dry fibers. One roller is attached to a compression spring that applies a uniform pressure. The other roller is attached to a step motor that controls rotation speed and torque. Two fiber-feeding components maintain fiber tension during travel; this is essential to ensure that the printing length is precise and accurate cutting. Fiber tension is maintained during the transition and also from the latter roller feed to the time of layering. During printing, the rollers move somewhat more slowly than the head, to maintain fiber tension.

Fiber-cutting is simple; system uses scissors with blades fabricated from hard durable steel. The cutter is driven by a servo motor placed on the head. To ensure accurate cutting of carbon fiber bundles, this has programmed repeat cutting sessions. During cutting, the fiber-feeding rollers periodically stop and then recommence rolling in the reverse direction. This increases fiber tension during cutting, ensuring that the cut cross-section is sharp.

Fiber-laying employed a set of rollers and a spring that imparted pressure and this is similar to the fiber-feeding system of ATL. The fiber is firmly held between the roller and the substrate. The roller is covered with a non-woven fabric (of defined thickness) that absorbed epoxy resin but not urethane. When a dry fiber is pressed to the epoxy-absorbing fabric, the epoxy infiltrated the dry fiber (this constituted printing); the wet fiber is printed on the substrate as the roller is actuated. The epoxy is a mix of liquid epoxy and liquid hardener. The fiber information is shown in Figure 7. The fiber material is selected roving type of fiber and based on these, the parameters for fiber laying and feeing parts are designed. Both the epoxy and the hardener are delivered via independent pneumatic actuators. The volume epoxy: hardener ratio, and their mass flows, are controlled by varying the pressures of the pneumatic feeder.

Tow size	Bobbin weight (*kg*)	Bobbin size (*mm*)					Case weight (*kg*)
		a	b	c	d	e	
12K	4	76	83	280	170	250	24

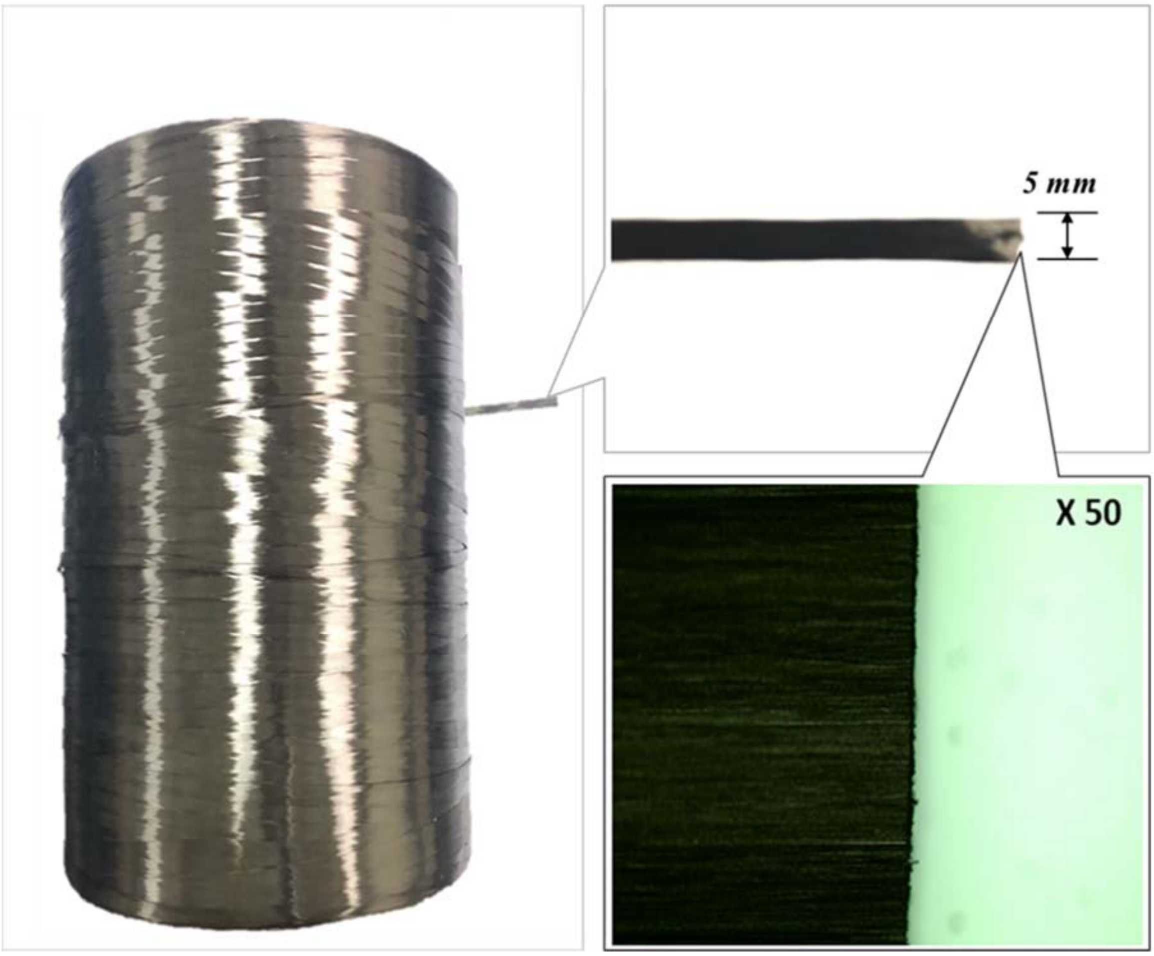

Figure 7 Bobbin information and magnified view of a fiber after cutting.

3.1.3 Epoxy feeding component

The other part is the chamber to control a certain amount of epoxy. The chamber has been designed to feed the exact amount of epoxy to the carbon fiber continuously. The insert angle of the camber is 55° and the end of trace angle is 15° which made the printing rollers grab and laid wet carbon fiber on the substrate in better conditions. The curvature of the camber path is constant which made carbon fiber go through the chamber with less twist. The chamber is composed of epoxy insert parts, bumps, scrapers, and containers. The entry of the epoxy insert part is 2 mm round shape and narrows down to 6 mm by 1 mm tetragonal shape to feed epoxy uniformly to carbon fiber. Five bumps on the path of carbon fiber help feed epoxy from the bottom side of the carbon fiber. Scrapers help remove excess resin and the excessive resin will be contained in the container of the chamber. Figure 8 shows detail the chambered information of chamber

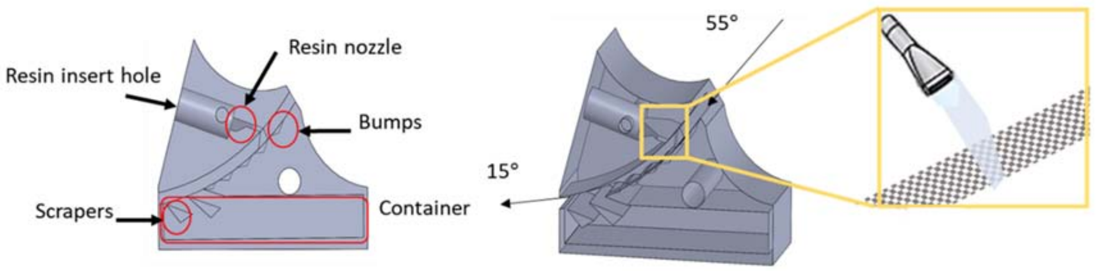

Figure 8 Design of chamber

The fiber volume fraction of the CFRP stands for a volume ratio of carbon fiber per carbon fiber with epoxy. Well-made CFRP has the fiber volume fraction of CFRP, normally between 50% to 60%. So, proposed printer is aimed to get 50% to 60% of fiber volume fraction and tested by feeding different amounts of epoxy. Epoxy is inserted so the ratio of carbon fiber volume per carbon fiber with liquid epoxy is 52 ~ 62%. However, in the curing process, there is the shrinkage of the matrix material. So, the fiber volume fraction of fabricated CFRP using this system is not that high. The two types of double repair specimens are designed and tensile tests are conducted. Fraction load is highest when the volume ratio of carbon fiber per carbon fiber with liquid epoxy is 62%. The result comes out that fraction load decreases as the ratio of epoxy decreases. If more epoxy is fed, the epoxy excessed and it makes cure longer that means it does not fit our printing system.

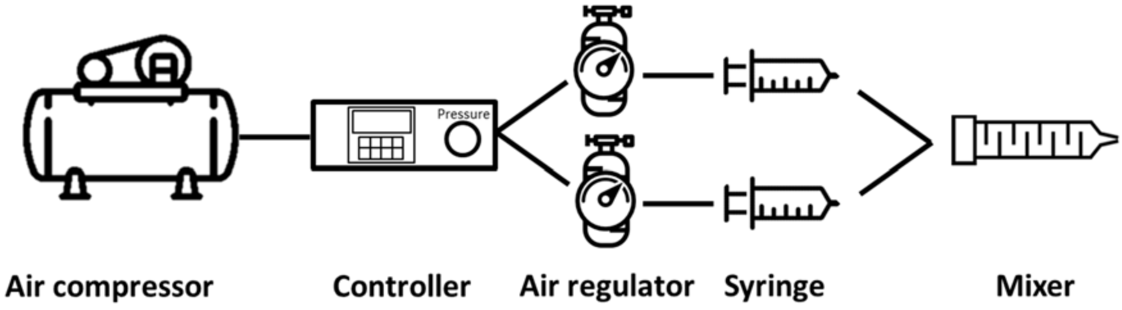

Figure 9 Schematic diagram of epoxy feeding system

3.2 Rapid curing system

3.2.1 Overview of rapid curing process

The conventional curing process of a composite is usually oven curing. In the conventional oven curing technique, the vacuum-bagged assembled samples are prepared as the procedure [59, 60]. Induction curing and microwave curing are studied hard for the non-contact heating process. Electrical or magnetic energy to heat materials that are electrically conductive such as carbon fiber [61]. However, still, this heating equipment and process require the additional process for curing because of curing time and pressure parameters. So, in this research, the Joule heating method is proposed as a rapid curing process. Although Joule heat requires direct contact for heating, using this characteristic, this module controls the pressure during heating fibers. The samples are cured at various temperatures and times. According to the result of the test, this study has reduced the curing time in the target area. This can apply the curing procedures are conducted within printing fibers, which means rapid curing with in-situ curing system is proposed. This can be contrasted with other heating methods where heat is generated in additional processes with oven, autoclave which require complex manufacturing for the repair process.

3.2.2 Modeling for rapid curing

For rapid curing, the important concept is to use carbon fiber as the heating element. Figure 10 Concept of heating model shows the concept of the proposed idea.

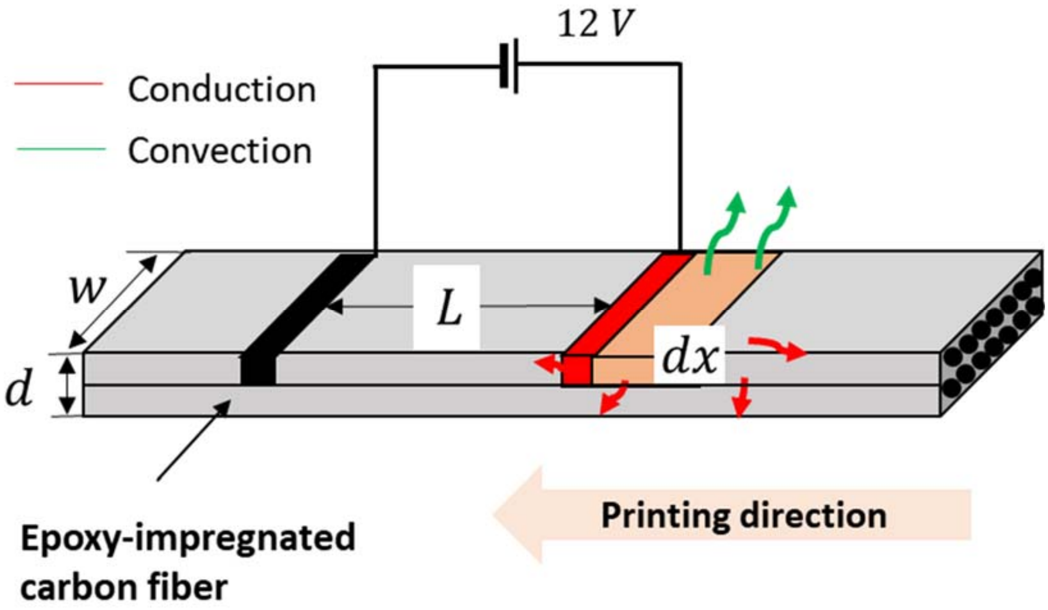

Figure 10 Concept of heating model

This idea is that carbon fiber generates heat via Joule heating then, cures mixed epoxy-hardener. To achieve this idea, there are some settings for the electrical-thermal model. At first, a short saturation time for the transition temperature of epoxy-hardener is required to use Joule heating. Second, define new material as "epoxy-impregnated carbon fiber" and to define this conceptual material 'rule of mixture (ROM)' is used. To optimize the length of heating element, L is called for the length of the carbon fiber. The micro area is defined for observing the heat flux caused by the Joule heating, convection, and conduction.

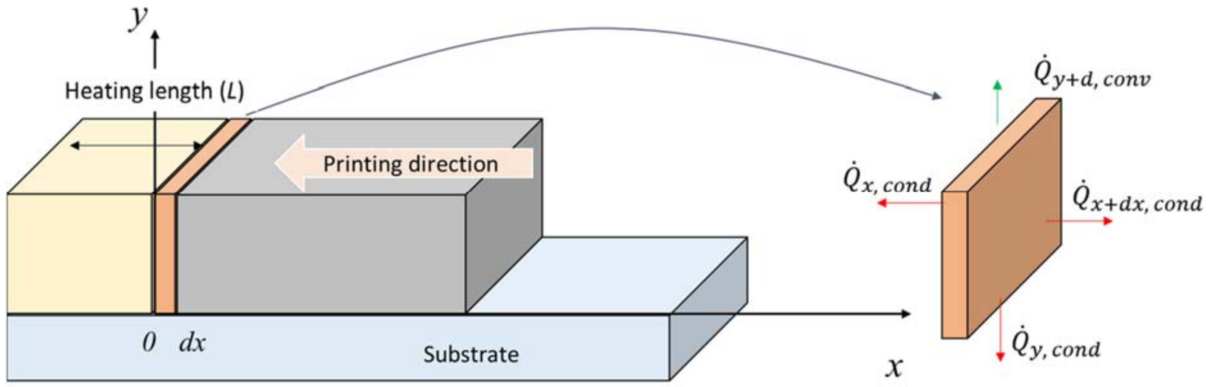

Figure 11 Detail heat transfer information

The detail heat transfer is shown in Figure 11. The starting point of the Joule heating area is defined as ‘0’ for displacement and ‘*dx*’ multiplied with the cross-section area of epoxy-impregnated carbon fibers can derive the microvolume for defining temperature change of epoxy-impregnated carbon fiber which means ‘*dV*’. After the definition of the microvolume for the heating element, the heat conduction to horizontal fibers, heat conduction to substrate and convection are considered in defining microvolume. In the case of steady-state analysis, based on the first law of thermodynamics, heat energy generated by electric energy can change to the required energy of curing of epoxy-impregnated fiber except for the energy loss from conduction and convection. This can explain in equation (3-1):

$$\dot{E}_{gen,\ electric} - \dot{Q}_{x,\ cond} - \dot{Q}_{x+dx,\ cond} - \dot{Q}_{y,\ cond} - \dot{Q}_{y+dy,\ conv}$$

$$= c\rho\,(dx\,d\,w)\frac{dT}{dt} \qquad (3\text{-}1)$$

where c, ρ in equation (3-1) shows the heat capacity and density of epoxy-impregnated carbon, respectively. To detail analysis of conduction, convection and heat generation, equation (3-1) can explain using temperature change rate (dT/dt) value in equation (3-2) :

$$i^2 dR - k_i(w\,d)\left.\frac{dT}{dx}\right|_x - k_i(w\,d)\left.\frac{dT}{dx}\right|_{x+dx} - k_i(w\,dx)\frac{dT}{dy} - h(w\,dx)(T - T_{envir})$$

$$= c_i\rho\,(dx\,d\,w)\frac{dT}{dt} \qquad (3\text{-}2)$$

where the conduction to horizontal direction is assumed quite insignificant and this is identified using test which is shown in Figure 11. So, based on this, governing equation (3-3) is:

$$i^2 dR - k_i(w\,dx)\frac{dT}{dy} - h(w\,dx)(T - T_{envir}) = c_i\rho\,(dx\,d\,w)\frac{dT}{dt} \qquad (3\text{-}3)$$

To the optimized length of a heating element according to temperature constraint, the equation can be rearranged in (3-4):

$$dT = \frac{i^2\, dR\, dt - k_i (w\, dx) \frac{dT}{dy} dt - h(w\, dx)(T - T_{envir})\, dt}{c_i \rho\, (dx\, d\, w)} \tag{3-4}$$

Based on this equation (3-4), classify the region when the displacement of dx is the inner region of the heating area which defined volume get electric thermal energy with heat energy loss from conduction and convection. The second region, could be call cooling, disappear the heat generation of electric energy. So, according to the region, the equation could be explained in (3-5) and (3-6):

Heating area (if x(i)<L)

$$dT = \frac{i^2\, dR\, dt - k_i (w\, dx) \frac{T(i) - T_{envir}}{d} dt - h(w\, dx)(T(i) - T_{envir})\, dt}{c_i \rho\, (dx\, d\, w)} \tag{3-5}$$

where,

cooling area (if x(i)≥L)

$$dT = \frac{-k_i(w\,dx)\frac{T(i)-T_{envir}}{d}dt - h(w\,dx)(T(i)-T_{envir})\,dt}{c_i\rho\,(dx\,d\,w)} \quad (3\text{-}6)$$

To integrate the parameter and plot temperature versus time graph, t(i) and T(i) are:

$$t(i+1) = t(i) + dt \quad (3\text{-}7)$$

$$T(i+1) = T(i) + dT \quad (3\text{-}8)$$

These equations can derive Figure 12 according to the length of the heating element from 8 to 14 mm.

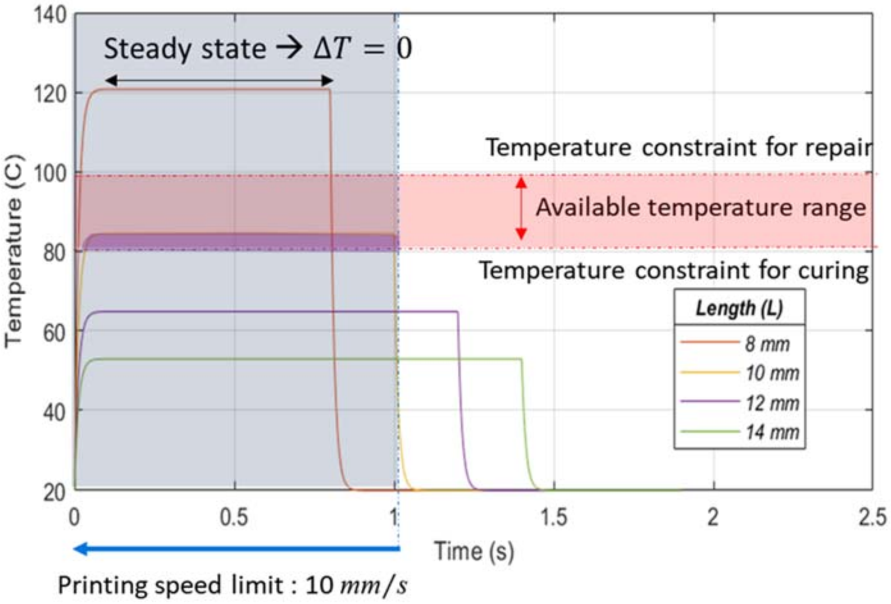

Figure 12 Heating length optimization

Figure 12 shows the when the length of the heating element is longer, the temperature cannot reach the target temperature which glass transition temperature of mixed epoxy-hardener. The developed automated fiber laying system has another constraint such as printing speed. The concept of this rapid curing system should be curing the epoxy-impregnated fiber during printing so, target temperature should be achieved in printing speed (lead of fiber). The last constraint parameter also the temperature is lower than 100℃ because the substrate could be distorted. According to the result of the governing equation about the heating model and constraint conditions in Figure 12, the parameters for rapid curing system fabrication are considered. The parameters which are determined during the design process are explained after this chapter.

3.2.3 Joule heating module

In this research, the printing system includes a rapid curing system. The epoxy selection for rapid curing is a very important issue. To control the degree of curing with temperature, various features of bisphenol A type epoxy are tested. Since strength and rigidity as an aero material are required, the resin (KFR 120, Kukdo chemical, Korea) and the hardener (KFH 163, Kukdo chemical, Korea) which can satisfy those conditions are chosen. This combination has secondary reactants to accelerate the overall chemical reaction process and this is sensitive to heat. The temperature is higher than the glass transition temperature, the activation energy goes low, then the reaction goes faster [66, 67]. However, excessive heat can affect the substrate also with a repair patch and it affects the crosslink density that means the strength goes down so proper condition should be selected based on an experiment.

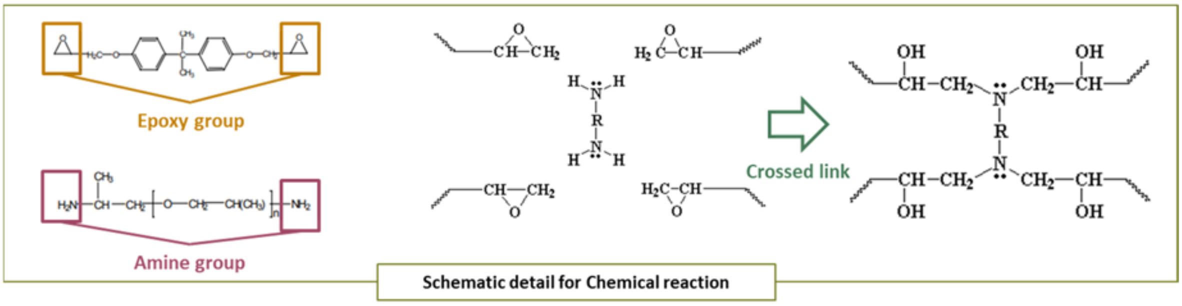

Figure 13 A schematic illustration of crosslink reaction between bisphenol A and hardener

So, using this characteristic of this combination, samples are prepared with the heating press and universal testing systems. The specimen is fabricated using 12-K (T700CA, Toray, Japan) carbon fiber and four-layered specimens according to ASTM standard. The reason using the heating press is the proposed carbon printer system also using the contact heating method (Figure 14) so reference samples also are prepared that method for proper comparison.

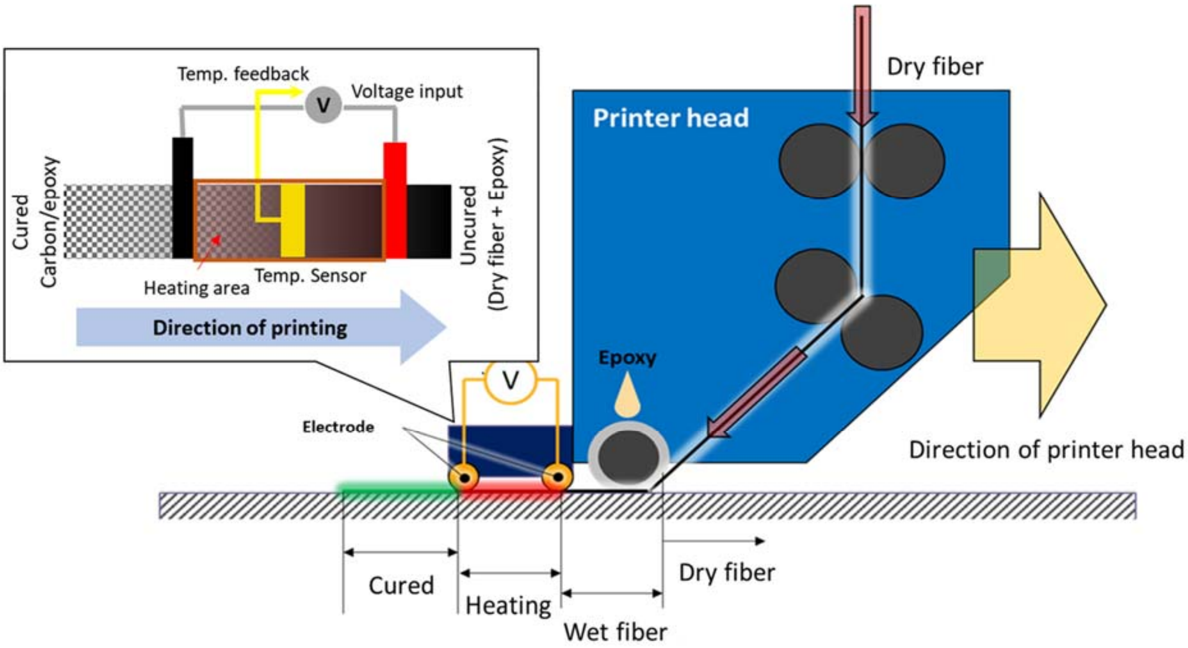

Figure 14 A illustration of the new carbon fiber printing system

These samples are fabricated using a vacuum bag with heat press the conditions of each sample are prepared. Heat press (D3P-35J, Dae Hueng Science, Korea) is set the pressure 5 MPa on samples. After fabricating samples, the universal testing system (Model 43.304, MTS, USA) has tested the coupons. Universal test system imparts force of up to 30 kN. Testing and repair method meet the ASTM D3039 and D3528 standards; non-tapered tabs are attached.

Samples are controlled the same pressure as 5 MPa which is usually the recommended parameter in the autoclave fabrication method [66]. To recognize optimized conditions between time and temperature, parameter study is conducted for these values as Table 3-1. Tensile samples are fabricated two kinds of UD such as 0° and 90° at different times and temperatures. After that, the coupons are cut as ASTM standard (ASTM D 3039). The detail result of the double lap test will be illustrated in chapter 4 with a cross-section of fracture happens in the middle of the coupon.

Table 3-1 The experimental condition and result of tensile test

Temp. Time	80℃	100℃	130℃
6 h	● Manufacturer reference		
1 h	●	●	
30 m		●	●
5 m		●	●

For this preliminary test, rough guide values are verified for shortening the time for curing. At first, before mentioned in the overview, tried to heat the fiber using frequency sources such as microwave, induction type. However, microwave source has a risk for humans and the induction system is not effective because of the feature as a bundle of fiber, which is cooling fast and the unconstrained amount of epoxy can transmit heat non-uniformly. Joule heating can heat locally, but fast. There is a study about fast heating using some epoxy with nanomaterials, which are nanotube or particles [68, 69]. The targeted system does not require a large area for heating so this research chooses a direct Joule heating system. Figure 15 shows the feasibility test setup for verifying heating times and heat flux.

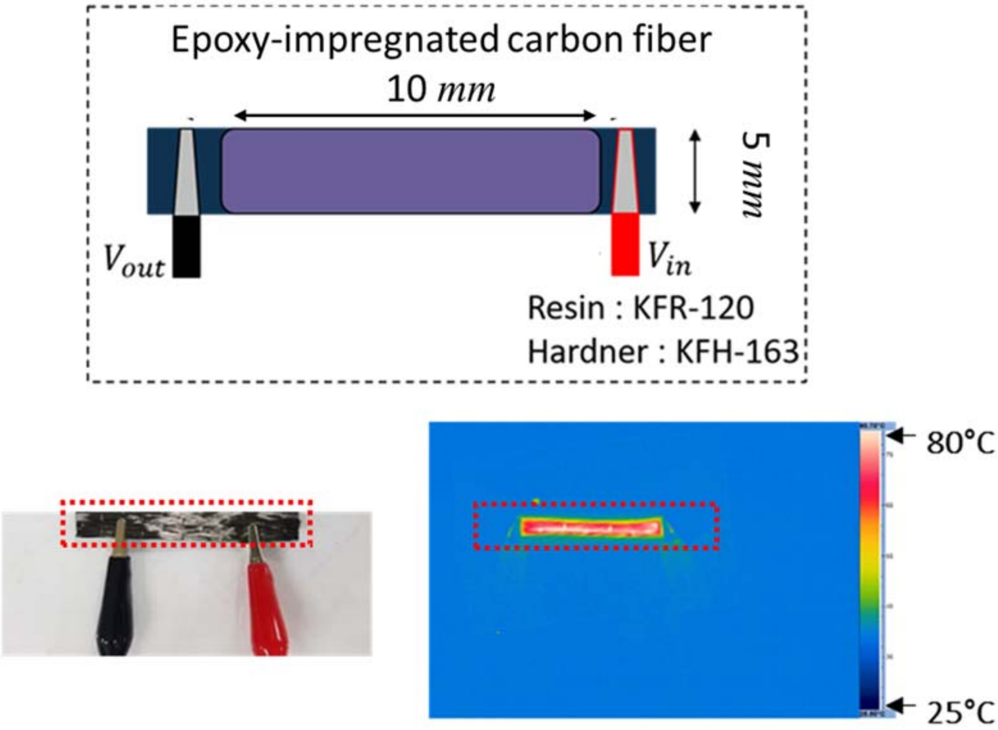

Figure 15 Schematic illustration and condition of feasibility test

In this setup, DC power use as power source. Using this is not enough to control the temperature of the fiber with epoxy because there is surplus heating from continuous source input. It caused temperature goes higher than the targeted temperature. This result shows the feedback system is required to compensate the surplus heat generation. The considered design parameters will be introduced.

3.2.4 Electric-Thermal feedback module

Based on the direct printing system, time for cutting into patch size is reduced. However, in the whole time of the repair process, the largest portion in the fabrication CFRP patch is the curing process. The rapid curing can reduce or remove this process. So, in Figure 16, using Joule heat with a feedback system is proposed and designed. The electrical characteristic of carbon fiber makes conduct electron between electrodes. Using this characteristic, electrical signals such as resistance, current, and voltage can match with thermocouple data and this can control the input source signals. Relay is the proposed trigger for input signal because of surplus heat, which is mentioned in the previous chapter.

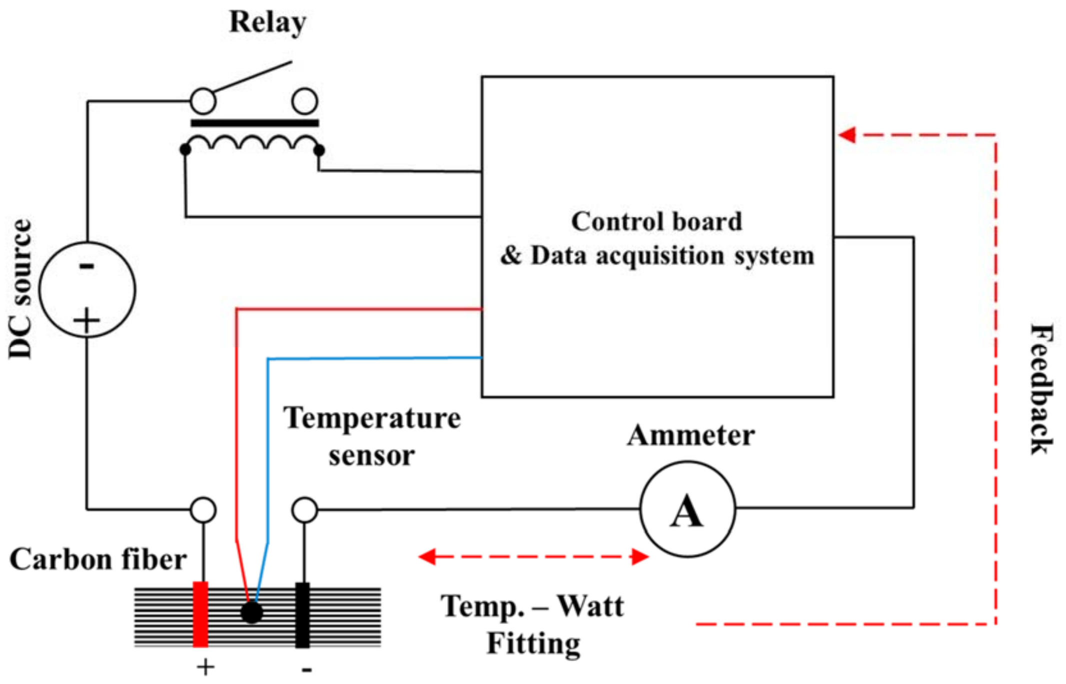

Figure 16 Schematic diagram of heating system

The actual configuration is shown in Figure 17. Data acquisition (DAQ) module (NI-6363, National Instruments, USA) has been used as trigger and controller for the relay system, current and temperature.

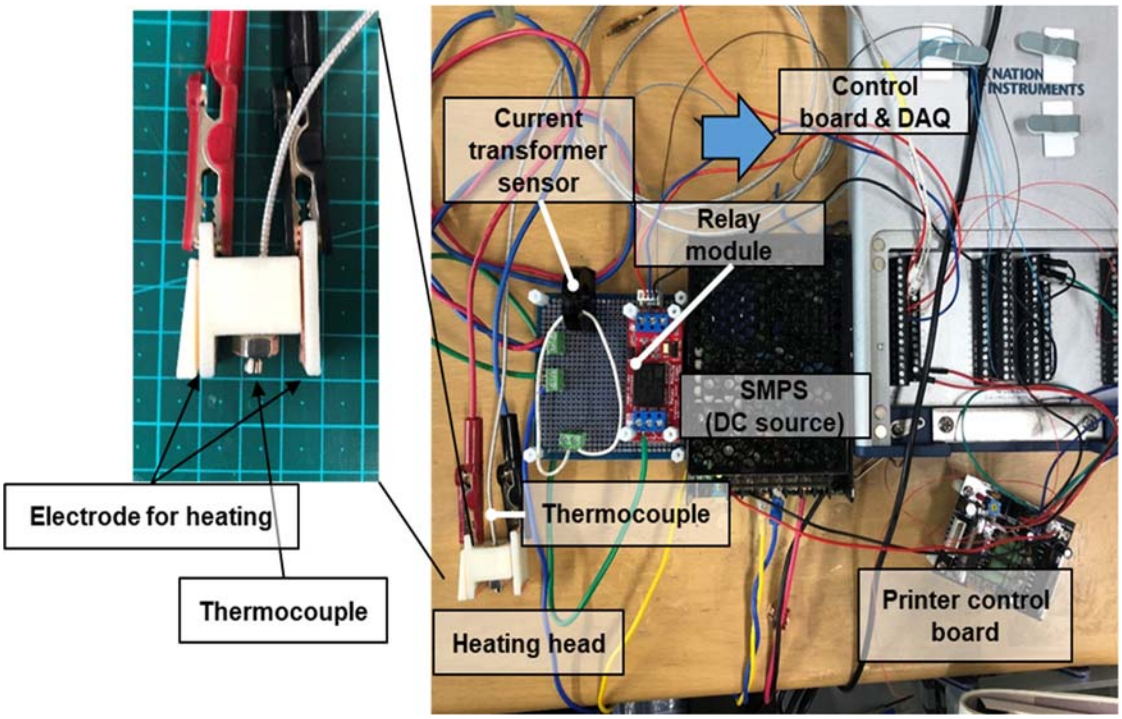

Figure 17 Configuration detail of designed heating system

The temperature of the curing parameter is tested based on the result which is shown in Table 3-1. The glass transition temperature of this combination which means mixture of the resin and hardener is 80℃ and target-time is a few seconds. Based on these three values fitting, our system controls the temperature on fiber for curing with the current which means Watt on between electrodes at the heating head. Before the feasibility test can find around 4 to 12 W can heat 10 mm of 12-K carbon fiber enough for curing in a few seconds. So, in this system. The power source is determined as 12 V DC switching mode power supply (SMPS). Using a relay trigger, the proposed system controls the duty and frequency of current that make electrical power 4 to 12 W. This value is controlled by data from the thermocouple between electrodes. Figure 18 shows the temperature is controlled during heating carbon fiber with the change of duty via the relay module. This feedback system is controlled by data from the thermocouple. Using this system, carbon fiber can get uniform temperature continuous during printing. The numerical model which is introduced from the previous chapter can set the parameters such as input voltage source and change of the resistance according to length. The result of numerical analysis can derive the parameters when the trigger turns on and off, and what temperature can cover the surplus heat which can cause repair defect.

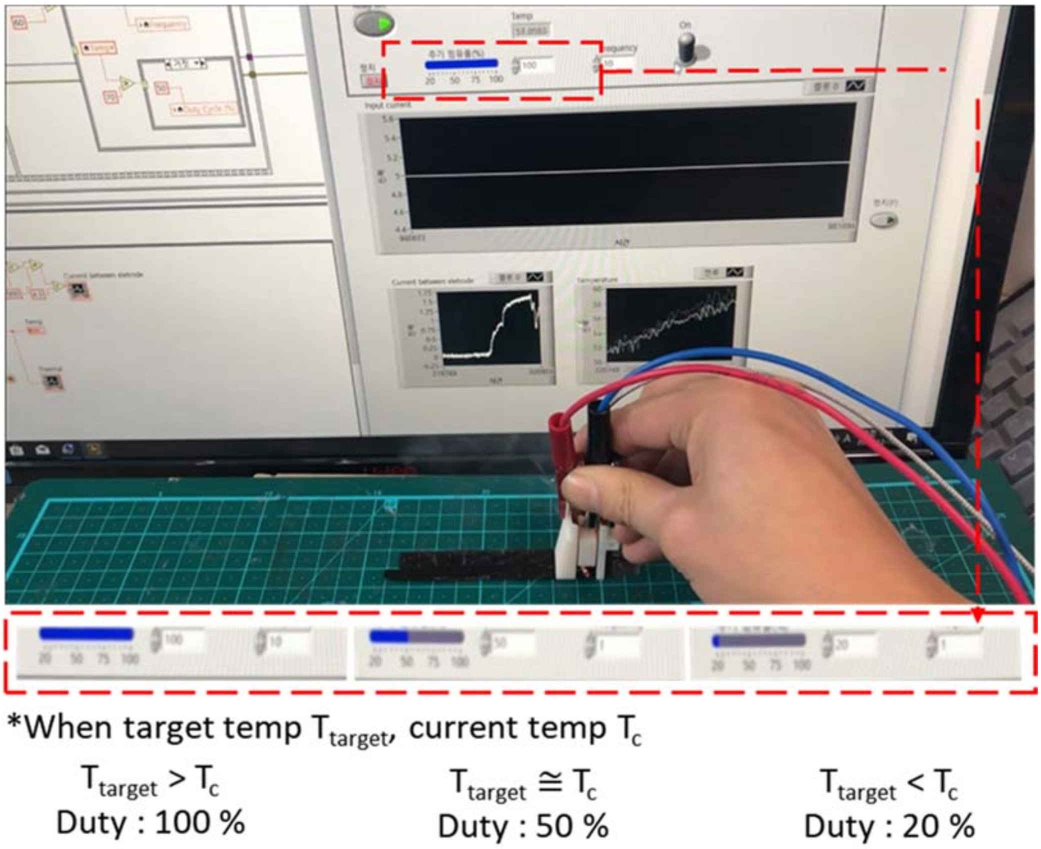

Figure 18 Temperature feedback using duty control

The last component is the jig for electrodes. Based on numerical analysis of the previous chapter, 10 mm-length-electrode jigs are designed and this maintains the distance between electrode with uniform pressure. Electrodes in contact with epoxy-impregnated fibers have been designed and fabricated as disposal components. These are designed as conductivity material with cover type of electrodes.

3.3 Highly sensitive sensor patch for SHM

3.3.1 Aerodynamically focused nanoparticle (AFN) printing

An AFN Printing system has been developed for room temperature particle printing system. The base concept of the AFN printing system generates and controls focused aerosol. First, from feeder nanoparticles applies pressure generated using excitation and purging of compressed air. Using this sequence, and aerosol is generated with nanoparticles and focused on using the structure of the nozzle.

The schematic diagram of the AFN printing system in Figure 20 shows the mechanism of nanoparticle printing. The focus of nanoparticles is determined by the air pressure and the nanoparticle size and weight.

AFN printing system is known for its more appropriate for the direct printing of metal and ceramic nanoparticles. In this research, silver nanoparticle (Sigma-Aldrich, particle size <100 nm) is used for printing sensors. Conventional printing silver nanoparticles evaluated in Figure 19. The various diameters are of the order of tens of micrometers.

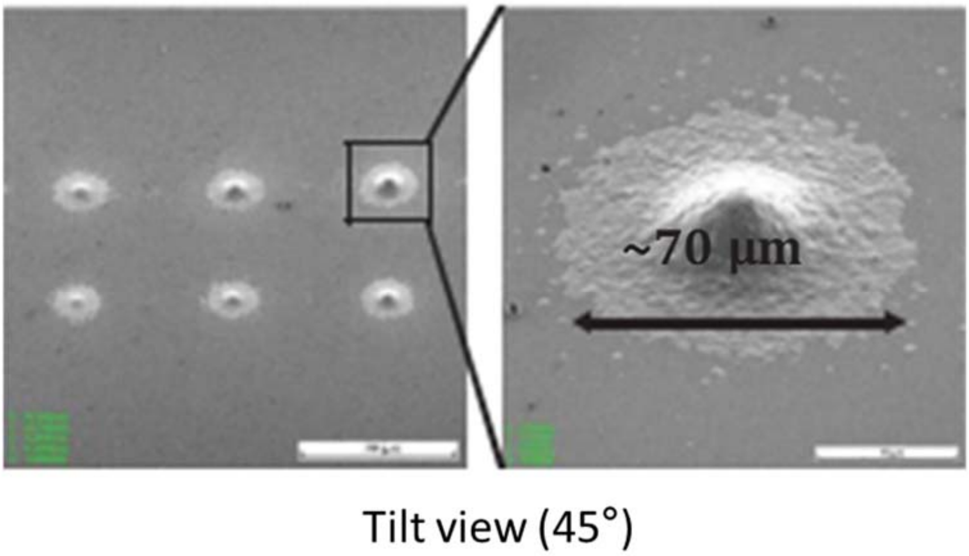

Figure 19 Silver structures printed by an AFN printing system

AFN printing system which is direct and dry inorganic nanoparticle deposition method in a low vacuum and room temperature condition is introduced. Besides, it does not require any post-process include in chemical etching or binding. Using porous properties of microscale conducted pattern fabricate by AFN printing system, the deposition mechanism of nanocomposites onto flexible substrates using the AFN printing system is also studied. Moreover, statistical analysis using the bivariate model is suggested and validated empirically.

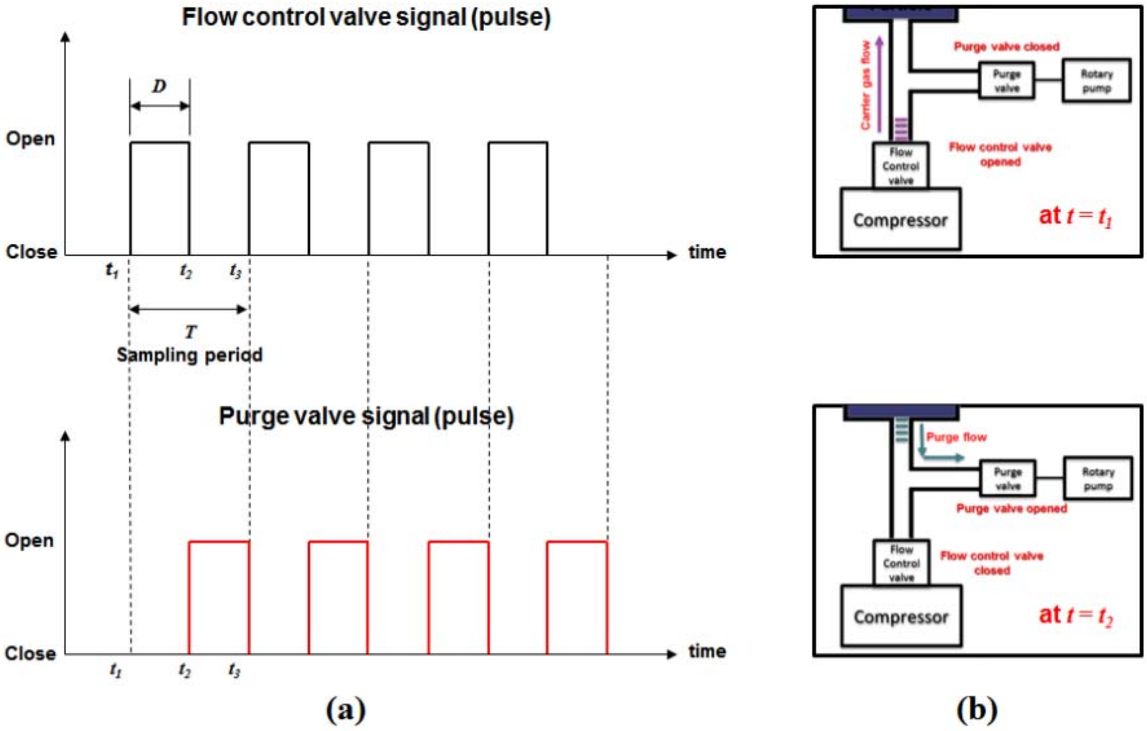

Figure 20 Schematic diagram of AFN printing system [70]

The configuration of AFN printing systems is shown in Figure 20. The printing system consists of a nanomaterials feeder, a vacuum chamber, and nozzle to create an aerosolized nanomaterials beam. Following shock-induced aerosol generation via control of excitation and purging time, aerosolized nanomaterials go and blow up to aerodynamic filter which occurs laminar aerosol flow. A transported aerosolized nanomaterial is aerodynamically focused when it is spurting out from the nozzle, and directly deposited onto a substrate. As nanomaterials are deposited by a high-speed impact with a substrate, AFN printing systems are suitable for direct printing of various inorganic materials without chemical bonding or heat treatment. Direct printing is a particularly efficient technique for the fabrication of microscale patterns such as strain sensors. Microscale porous pattern composed of nanomaterials can be freely printed as desired regardless of geometry and design. Also, patterns can be repaired or reconfigured when necessary, which overcomes the limitations of conventional processes such as laser ablation or photolithography. Pattern width can be controlled by regulating the scan time of the AFN printing process which also enables the control of porosity inside the printed pattern as shown in Figure 20. A charge-coupled device (CCD) cameras (EO-0813C, Edmond Optics, USA) is used to measure the pattern width while AFN printing process. Since the porosity of the printed pattern is a dominant factor in the sensitivity of the nanocomposites sensor, AFN printing is used to fabricate strain sensors with high sensitivity in this study.

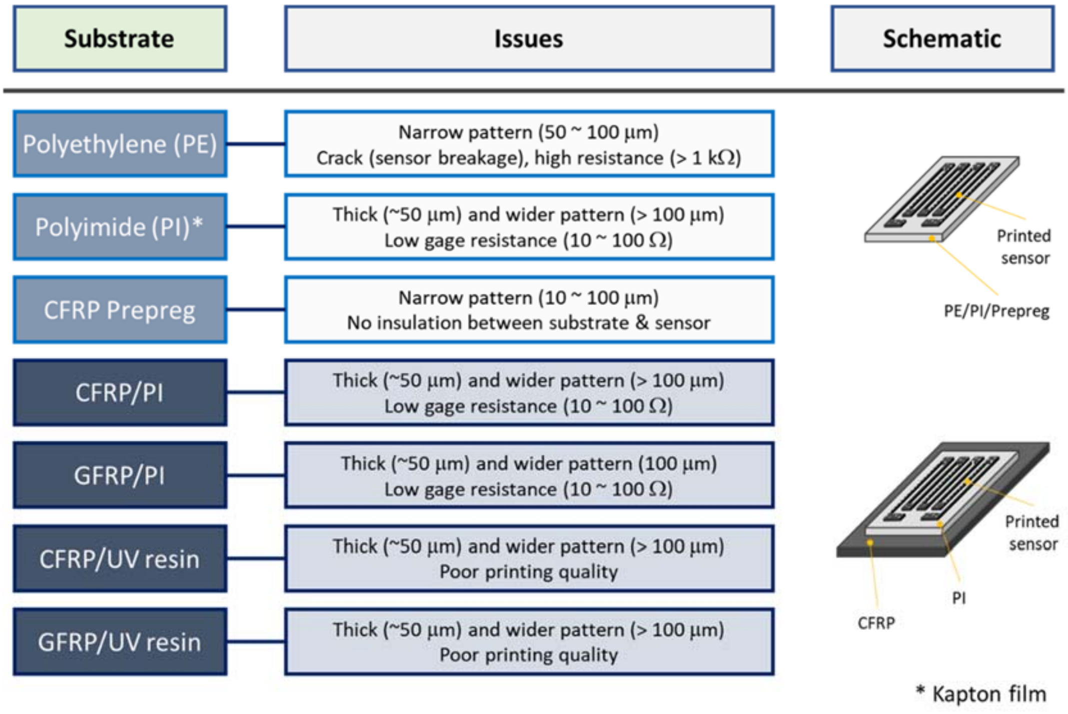

Substrate	Issues
Polyethylene (PE)	Narrow pattern (50 ~ 100 μm) Crack (sensor breakage), high resistance (> 1 kΩ)
Polyimide (PI)*	Thick (~50 μm) and wider pattern (> 100 μm) Low gage resistance (10 ~ 100 Ω)
CFRP Prepreg	Narrow pattern (10 ~ 100 μm) No insulation between substrate & sensor
CFRP/PI	Thick (~50 μm) and wider pattern (> 100 μm) Low gage resistance (10 ~ 100 Ω)
GFRP/PI	Thick (~50 μm) and wider pattern (100 μm) Low gage resistance (10 ~ 100 Ω)
CFRP/UV resin	Thick (~50 μm) and wider pattern (> 100 μm) Poor printing quality
GFRP/UV resin	Thick (~50 μm) and wider pattern (> 100 μm) Poor printing quality

Figure 21 Parameter study result of AFN printing

The printing qualities onto various substrates, including GFRPs and CFRPs, are investigated, for the prototyping of the printed nanoparticle strain sensors onto composites. The sensors are designed similar to the commercial strain gauge, with thin and long patterns in the longitudinal direction and thick and short patterns in the latitudinal direction. It helps not only to improve sensitivity in the longitudinal direction but also to reduce the effect on deformation in the latitudinal direction. The designed sensor has 8 lines in the longitudinal direction with a length of 7 mm.

3.3.2 Highly sensitive strain sensor

The strain of CFRP is not much bigger than commercial metal materials so highly sensitive strain sensors are proposed via the AFN printing system. Using this system, the sensor is designed using nanoparticles as materials. The characterization of particle sensors, such as the tunneling effect, can make a change of resistance amplified. This effect makes the proposed sensor is able to measure micro-strain of composite materials which is not easy to measure via a commercial strain sensor.

To print continuous line patterns, the feed rate of printing and the density of aerosolized nanocomposites must remain at a specific level. As the density of aerosol is controlled by time-scaling of excitation and purging of compressed air, optimizing process parameters is important to fabricate patterns as desired. Figure 21 shows the process parameters used in the AFN printing process for this research. Nanomaterials are carried by air driven by pressure difference between purging time and source chamber controlled by excitation time. In this study, pressure of the source and chamber remain at 1,000 Pa and 400 Pa each. Excitation time is the time to blow air into the feeder and purging time refers to the time taken for the air to escape from the feeder.

Table 3-2 Process parameters for AFN printing

Parameters	Values
Source pressure (*Pa*)	1,000
Chamber pressure (*Pa*)	400
Excitation time (*msec*)	10
Purging time (*msec*)	90
Feed rate (*mm/s*)	0.2
Distance between substrate and nozzle (*mm*)	1
Carrier gas	Air

Generally, printing on the composite structure is more difficult than the other hard substrates, such as metal or silicon substrate, because the printing characteristics might vary on the polymer resin used in the composite structure. In this study, the printed strain sensors with a backing layer on the top of the GFRPs and CFRPs are presented for qualitative comparisons of the results.

Focused on the control of the pattern width and height, the selected excitation valve timing is 40 ms and the stage speed is 10 μm/s. A representative printing demonstration (in-situ observation of the nanoparticle printing) is shown in Figure 22 (a) In-situ image captures Silver nanoparticle printing. (b) Detail dimension of the printed strain gauge pattern. (c) Schematic illustration of the specimen geometry onto the substrate. (d-e) Printing result of the strain gauge pattern onto PE film with its magnified image. Printing result of the strain gauge patterns onto (f) PI film and (g) CFRP prepreg. Strain gauge pattern with narrow lines (around 50 μm width) is printed successfully. Figure 22 (a) In-situ image captures Silver nanoparticle printing. (b) Detail dimension of the printed strain gauge pattern. (c) Schematic illustration of the specimen geometry onto the substrate. (d-e) Printing result of the strain gauge pattern onto PE film with its magnified image. Printing result of the strain gauge patterns onto (f) PI film and (g) CFRP prepreg. (b-c) show the pattern dimensions and its 3-dimensional geometry, respectively. Figure 22 (d) captures the optical image of the printed strain sensor (onto the PE film) and the magnified image of the printed line, taken by the optical microscope is presented in Figure 22 (e). The same strain gauge patterns are printed onto PI film (Figure 22 (f)) as well as the CFRP prepreg (Figure 22 (g)).

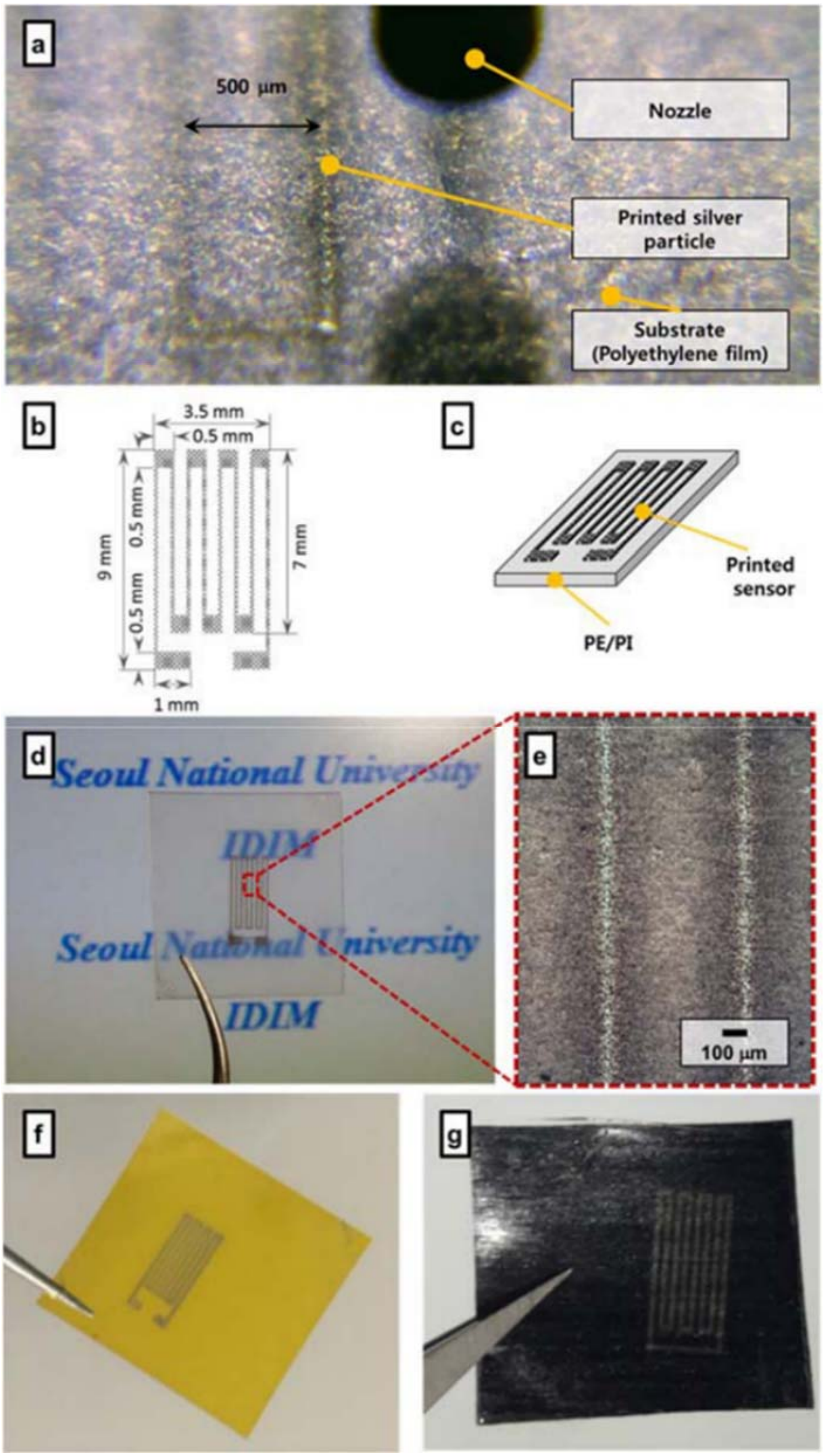

Figure 22 Printing demonstration and detail figures of proposed sensor

3.3.3 Design of sensor patch and communication system

At first, RFID tag with AFN printed particle strain sensor is proposed and studied. However, the resolution and sensitivity of this tag sensor are not enough for measuring composite properties. To overcome the above limitations, two candidates using radio frequency identification (RFID) technology are proposed to enhance the usability of fabricated sensors with repaired CFRP. RFID technology is one of the low-cost and fast communication technologies which is appropriate in universal local communication include automobile and airplane.

Passive RFID tag was tried using the AFN printing system with a strain sensor. This method has its advantages of reducing additional costs for a manufacturing process, connection and alignment of two different electronics. In addition, the possibility of influencing repaired CFRP is also reduced as the size of the entire system becomes dense. LC resonance-based RFID tag was printed but working between 1.3 GHz to 1.7 GHz. However, it has a relatively low sensitivity of about 0.6 as a gauge factor in comparison to commercial strain gauge with 2.0 as a gauge factor. It was considered that it would be unreasonable to use it in CFRP with a small difference in strain.

So alternative methods, RFID packaging systems composed of commercial modules are connected to a fabricated highly sensitive strain sensor. Using this method, the advantage of the high sensitivity of 1,000 based on the gauge factor of the developed strain sensor is achieved. Furthermore, the reliability of the entire system can be increased by utilizing commercial products. The proposed system and below show compactly design the entire system with commercial electrical modules. So, in this research, the conductive patterns which are printed using mentioned silver nanoparticles and the aerodynamically focused system can make various conductive patterns to be used for the strain sensor. Furthermore, the sensitivity of the printed nanoparticle in small dynamic signal measurements using mechanical cracks to enhance, data demonstrated that proposed strain sensors with its highest linear sensitivity of 1,056 and the vibrating signal of the sensor are demonstrated very small.

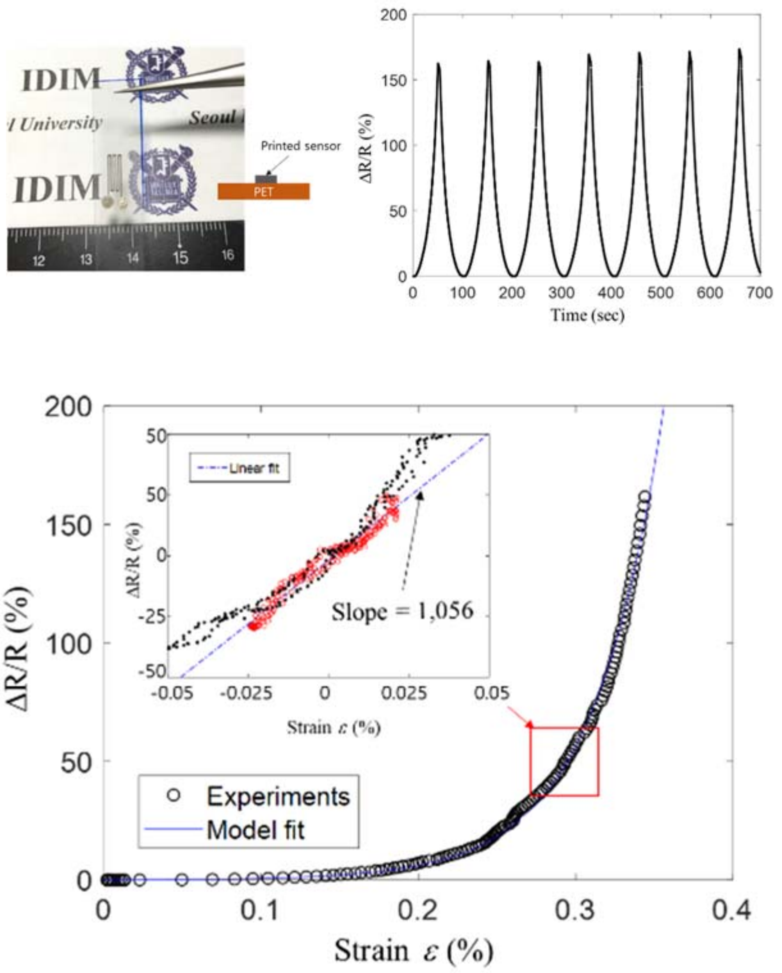

Figure 23 AFN printed AgNP sensor and its performance test

However, the bulky and complex data acquisition system is required for the measurement of the electrical signal of the AFN printed strain sensor. So prepared strain sensor is one of the passive-resistive type strain sensors with the external power source and connected electrical wires are needed to measure the change of the signal of stain. In general, external electrical systems connected to sensors are not only hard to directly install but also one of the major reasons to decrease the mechanical properties of repaired CFRP or aircraft stability.

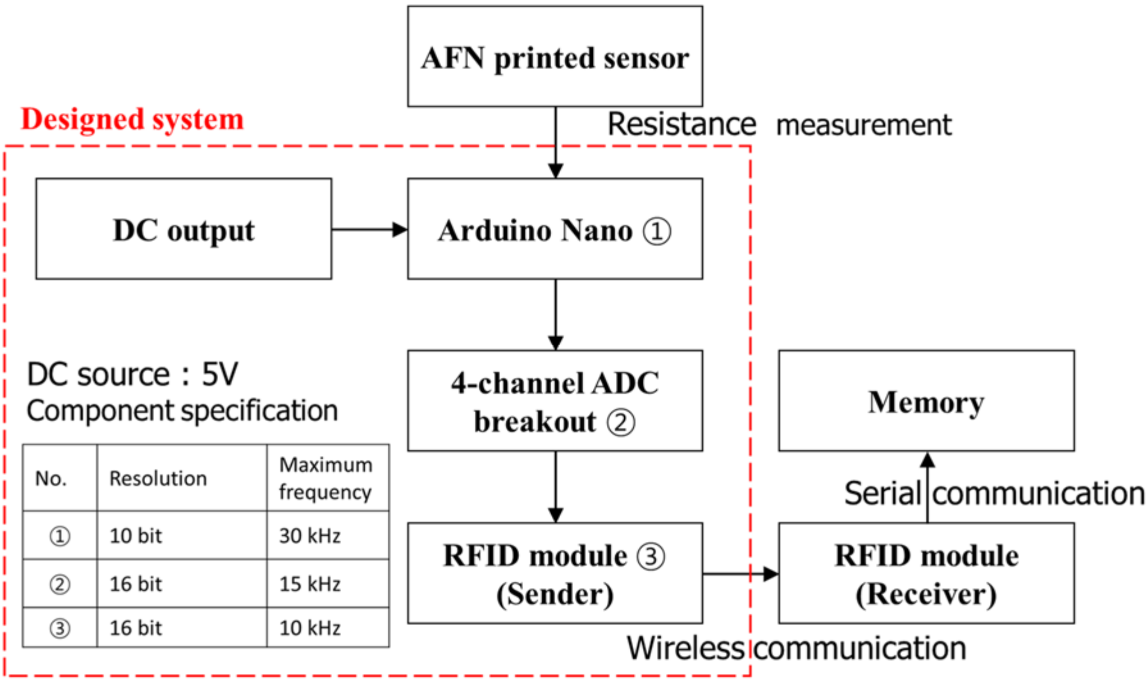

No.	Resolution	Maximum frequency
①	10 bit	30 kHz
②	16 bit	15 kHz
③	16 bit	10 kHz

Figure 24 Schematic diagram of designed circuit

RF communication is used to receive data wirelessly from the sensor manufactured using AFN. The advantages of RF communication are low power and a wide range of communication. In order to use RF, the smallest RF module is used. The specifications of this module are as follows:

Table 3-3 Specification of communication module

Component	Features
Frequency (*MHz*)	920.3 ~ 923.3
Data rate (*kbps*)	5
Dimension (mm^3)	22 × 19 × 3
Interface	I2C, GPIO, UART, ADC
Weight (*g*)	5

According to the specifications of this module, data can be sent and received once per second. To overcome this phenomenon, the system is improved using specific coding, which can collect data at intervals of 25 ms and send them at once. In addition, in order to make the most of the 5-kbps communication speed, the coding is changed to transmit only the initial value and after these data changes per second. By this improvement, 15 data reliably can be received per second.

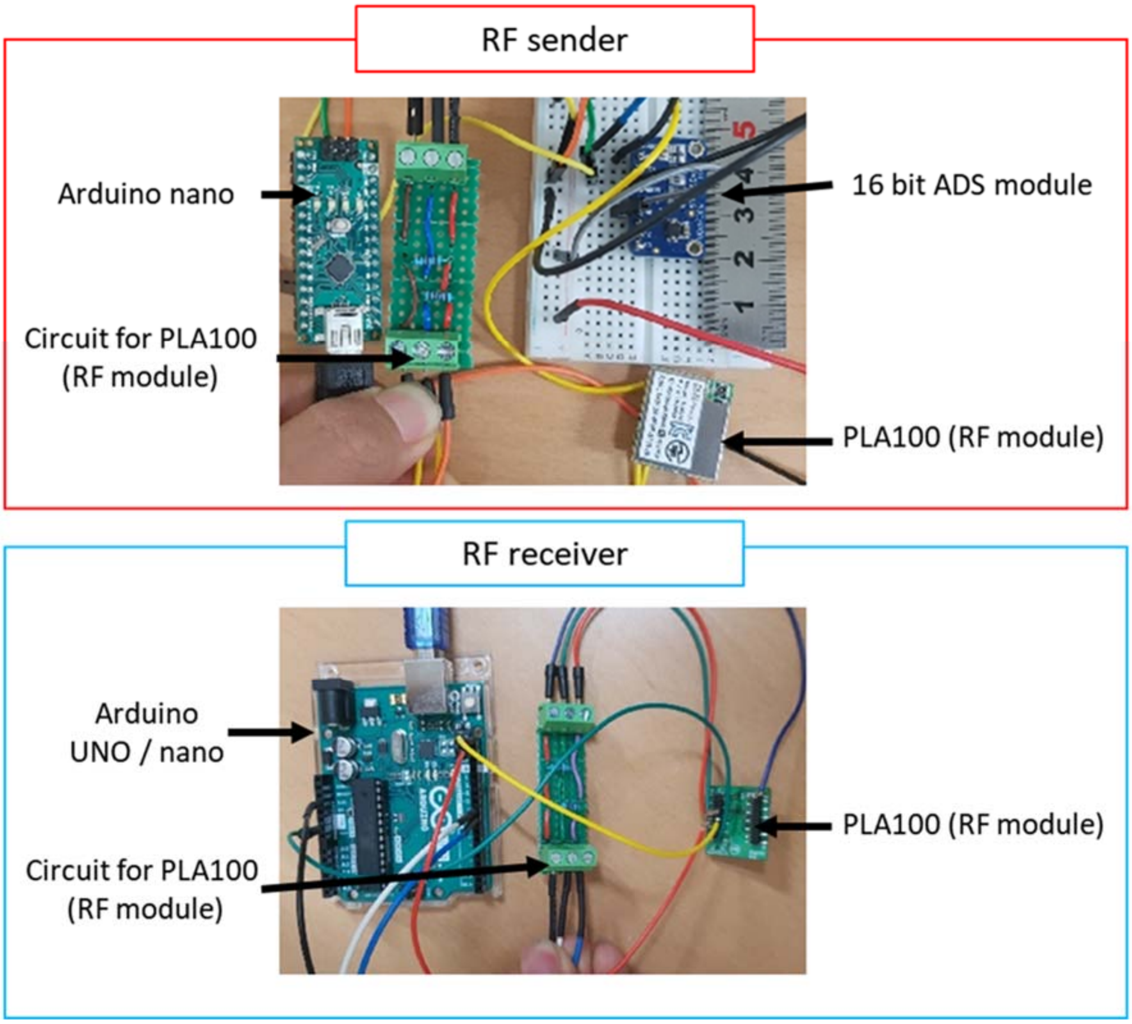

Figure 25 Simple RF module configuration

PCB circuit is used for sender configuration because of the miniature. The speed of data transition is a very important issue for resolution. Because the printed sensor is very highly sensitive but, if the resolution of communication is not enough to send, Missing data could occur and this makes users misunderstand of the life cycle of the printed repair patches.

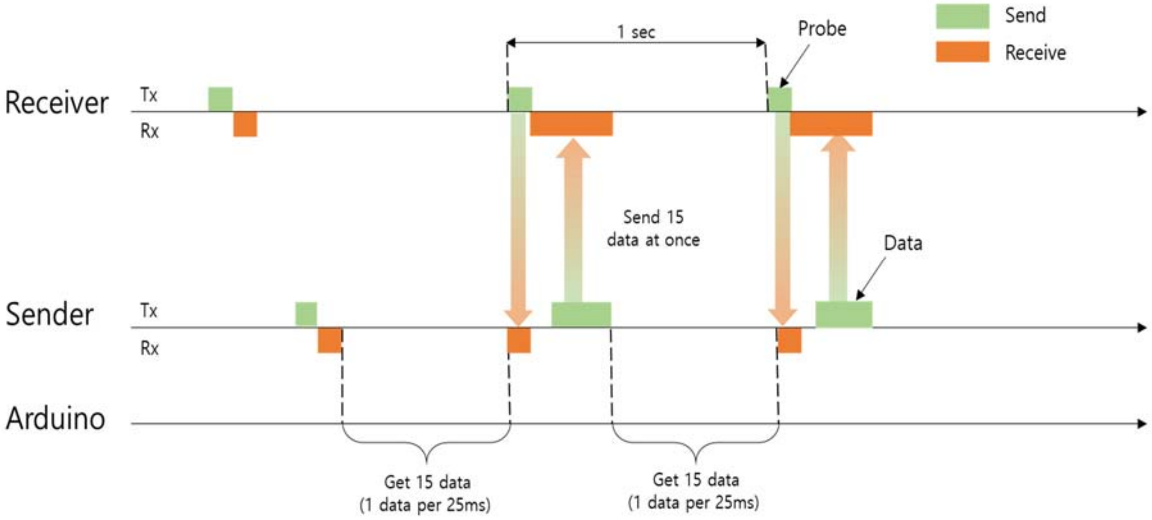

Figure 26 Schematic diagram of communication sequence

So, in order to know the time of each data, the operating time is recorded, which is the duration since the communication began. The operating time is tagged with a set of data received. Because each data is 25 ms apart, the time of each data can also be calculated if the operating time of the last data is known. So, to sum up, the time value of all the data is recorded.

Chapter 4. Evaluation

4.1 Evaluation of printed sample

Testing procedure to assess the quality of the repair, tensile tests according to DIN EN ISO 527-4 are conducted. Samples are cut into 250 mm × 25 mm specimens for testing. Testing is executed with a free patch length of 150 mm. At least five samples of each experiment had to be tested. By comparing the tensile strength and stiffness of the parent sample with the repaired samples the residual strength and residual stiffness could be sustained.

Sample preparation featured the following steps. A three-axis stage (OSMS 26-300, Sigma-koki, Japan) with a pivot allowing manual rotation is employed. The motors and pneumatic drives are connected to the data acquisition board; this allowed both control and feedback. The resin epoxy and hardener with a 12-K continuously roved dry fiber are used. The stiffness and fracture load of samples repaired via hand lay-up and the printer are compared. The tensile test specimen is a simple beam with the attached tabs; this met the ASTM D 3039 construction standard and the D3528 repair standard. When comparing repairs afforded by hand lay-up and the printer, the parent laminate (substrate) is cut into halves and re-joined using the two repair methods. The specimen is 12-K CFRP $[0/\pm45/90]_s$; this is a symmetrical carbon fiber with eight laminations. All samples that are repaired are prepared from entire CFRP plates and their dimensions are standardized; all samples are then cut into half prior to joining. Double lap joints are fabricated. Four layers of 12-K unidirectional carbon fibers are attached to either side, and they adequately covered the pre-existing layer. The gaps between cut specimens are 0.3 mm. Figure 27 presents the details.

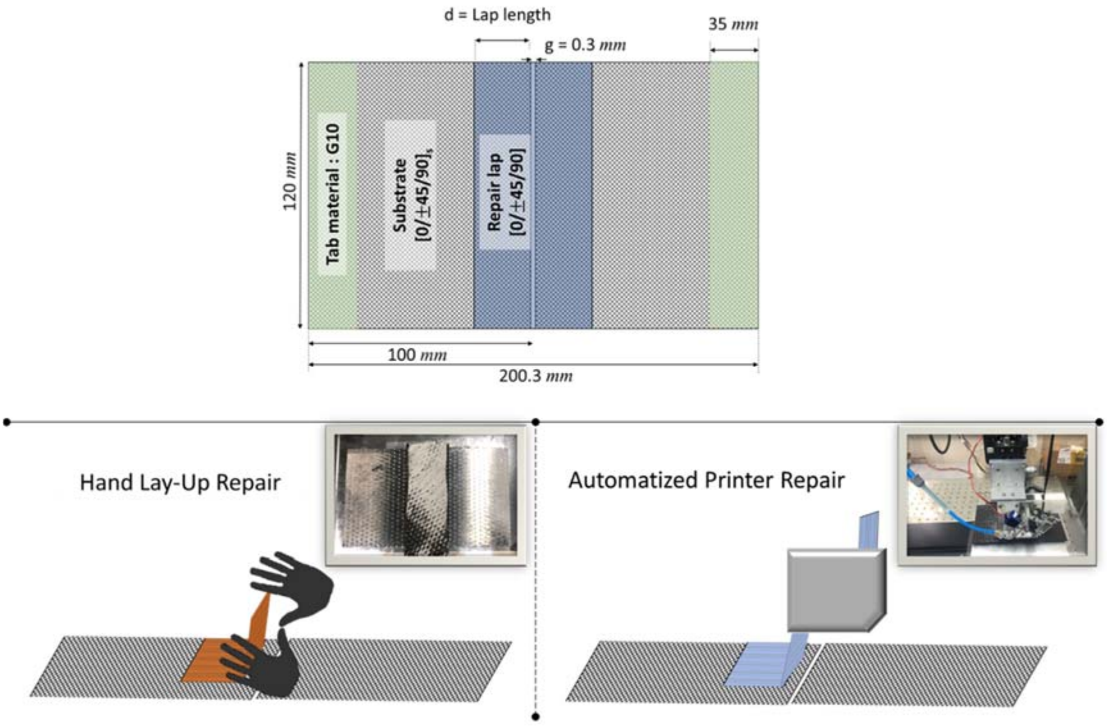

Figure 27 Schematics of the specimens used for tensile testing and those repaired using the two different methods

Figure 28 presents the fabrication processes; the upper panel shows how the printing facilitated thickness control. We attached a temporary support that prevented gap-widening between the plates, and a bleeder material, during upper-layer printing; the entire structure is then flipped with maintenance of the flat surface. During hand-lay-up repair, 12-K carbon fiber fabric is cut to match the planned layers and attached via epoxy resin. On the other hand, during the printer-repair, our system printed 12-K roving fiber in Table 4-1. There is no need to mix the epoxy with hardener and cut fabric into the planned layer size but code the printing trace. All specimens repaired using the printer and via hand lay-up are placed into identical vacuum bags containing molds. The mold prevented bending during vacuum-bagging. The information about raw materials, conditions of pressure and curing time is shown in Table 4-1.

Table 4-1 Materials and cure condition

Fabric information		**Density ($g\ /\ cm^3$)**	**Filament Diameter (μm)**
Base materials	T700G 12K (TORAYCA, Japan)	1.8	7
Hand-lay-up repair materials	T700G 12K (TORAYCA, Japan)		
Printer repair materials	AKSACA 12K A-42 (AKASACA, Japan)	1.78	
Matrix information		**Viscosity (cps)**	**Color (Gardner)**
Resin	KFR – 120 (Kukdo chemistry, Korea)	900 ~ 1100	0.5 Max
Hardener	KFH – 163 (Kukdo chemistry, Korea)	5 ~ 50	
Tab information		**Density ($g\ /\ cm^3$)**	**Flexural modulus (N / cm^2)**
Glass fiber sheet	G10 (Leson, China)	1.9	24000
Cure condition information			
Cure temperature (℃)	80		
Pressure (MPa)	5		

Five panels each are prepared according to the types of samples for the experiment. Each panel cut into five or more specimens. In Figure 28, the process of sample preparation is illustrated using developed printing system. First, printer placed epoxy-impregnated fiber on one side of cracked plates. The second, temporary support are placed for printing the other side. After that, there is the process for curing which means vacuum bagging with heating press. The same curing method and conditions are prepare for comparison between conventional vs. printed repaired. Finally, specimens subjected to hand lay-up and printer repair, and control non-damaged specimens, are prepared as shown in the lower panels of Figure 28.

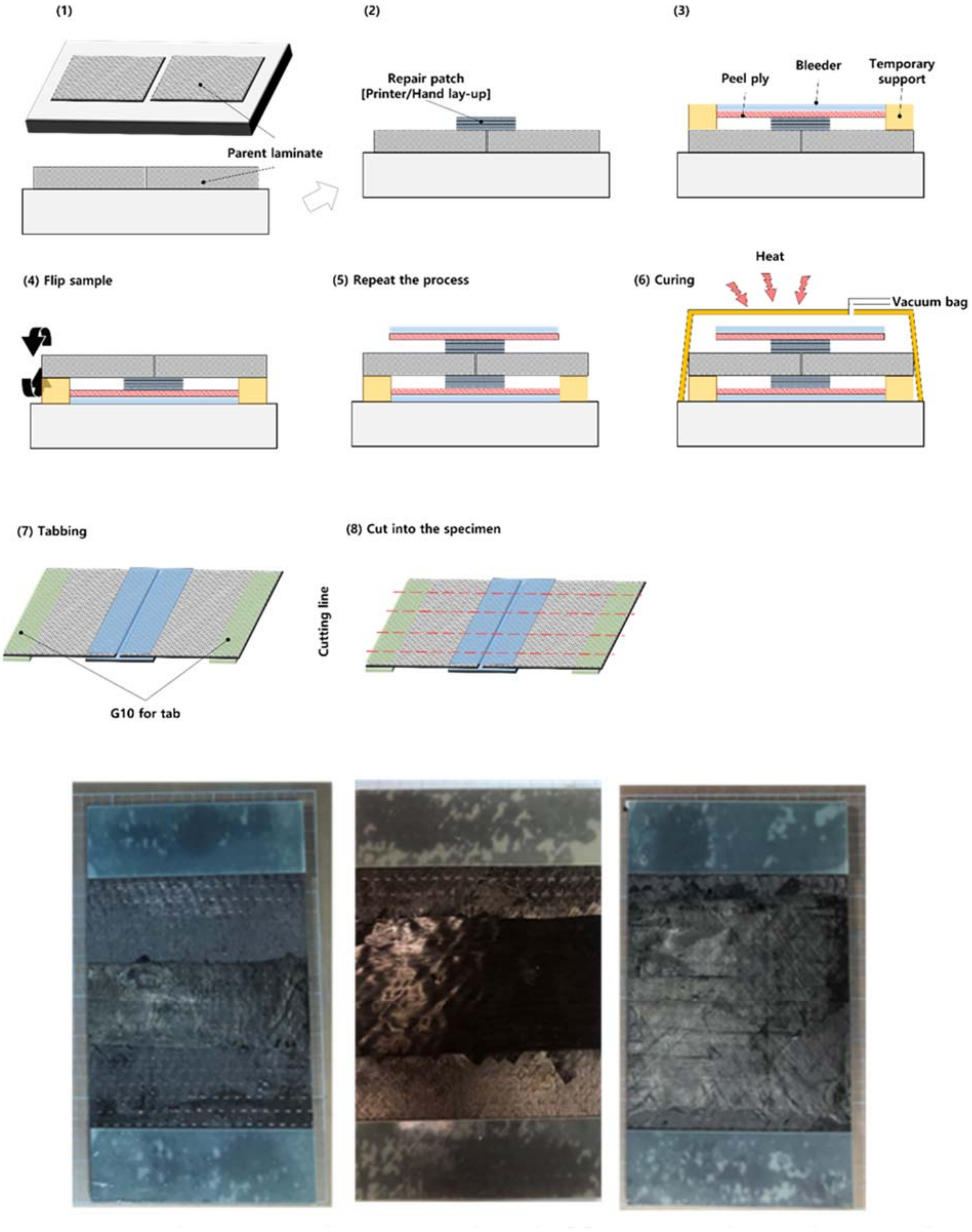

Figure 28 Schematic of printing and specimen preparation

Simple tensile tests are performed on five or more samples of each type via the universal testing system (Model 43.304, MTS, USA) imparting a force of up to 30 kN. Figure 29 presents the dimensions of the fabricated samples based on ASTM D3039 and D3528 standards.

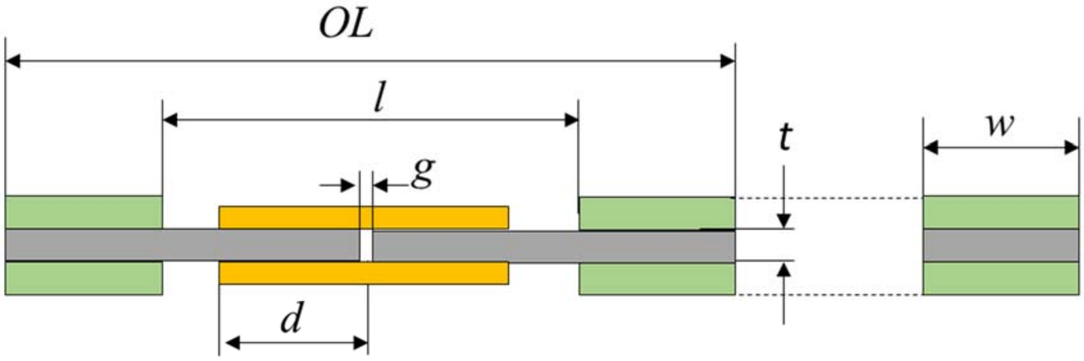

	Dimension [mm]
Lab length (d)	12.5 / 25 / 50
Overall Length (OL)	200
Test length (l)	150
Gap (g)	0.3
Width (w)	20
Thickness (t)	1.9

Figure 29 Tensile test setup and prepared sample with different lap length

The result of the test is shown in Figure 31. The recovery rate is defined in Table 4-2. Based on this result, same conditions and different repair method, developed printer improve the quality and the repair repeatability.

To explore why printer-repaired samples had similar or higher fracture load, fractured samples are cut (using a diamond cutter) and polished, and the cross-sections are examined. The cut sections included all repair patches. Figure 30 presents the cross-sections of two types of samples. Because the original CFRP and the hand-lay-up repair patch are created using an identical, unidirectional carbon fabric, the cross-sections reveal identical layer compositions and structures (as expected). However, the structures of the printer-repaired layers differed; the Second row of Figure 30 presents cross-section of the fracture areas. Printer-repaired samples have only uniform fibers laminates or boundaries for different angle ply. Hand-lay-up-repaired samples have the binder, clear boundaries between layers and voidages.

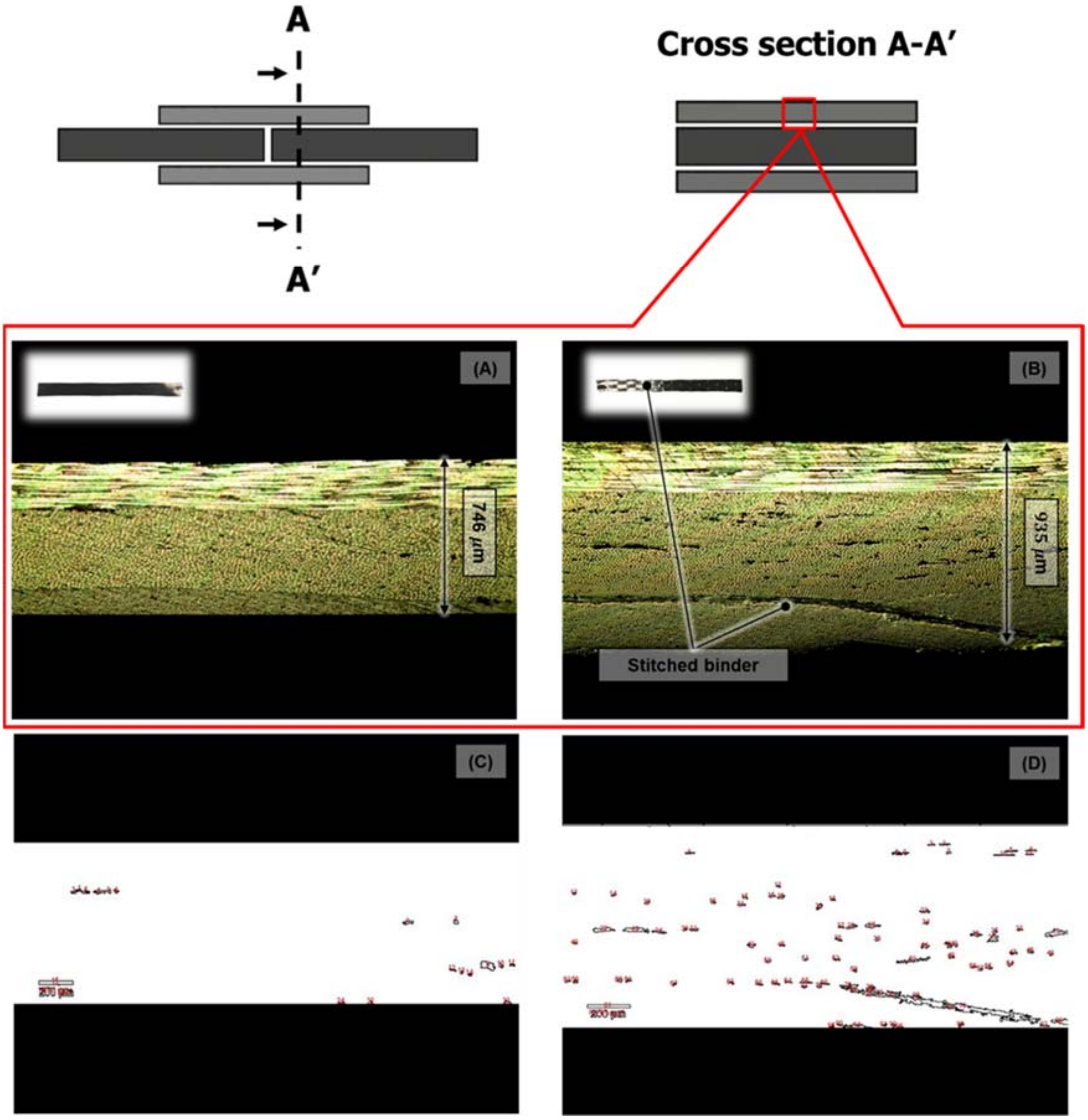

Figure 30 Magnified views of cross-sections of fractured sample and defects highlighted via image processing

As shown on the (A) of Figure 30, a printer-repaired sample is devoid of cracks in a cross-sectional view, and also free of visible defects that might increase the stiffness. This is because printing featured fiber layering under constant pressure. Direct fiber layering using roving carbon requires no additional materials (such as binders) to maintain fabric shape; printer-repaired CFRP exhibited a clean cross-section. The thickness of the repaired layer is uniform (746 μm), attributable to the use of direct printing. As shown on the (B) of Figure 30, the layer boundaries are clearly evident, as are void induced by the use of binders, and spaces lacking fibers. The hand-lay-up-repair sample is not of uniform thickness and thicker than printer-repaired samples (935 μm); thickness varied by binder layer direction. Based on this, the volume fraction of each type of repaired sample could be discussed. Fiber volume fraction (V_f) is calculated by using the following equation (4-1) [71]:

$$V_f = \frac{(w_{cf}/\rho_{cf})}{(w_{cf}/\rho_{cf}) + (w_m/\rho_m)} \tag{4-1}$$

here, w_{cf} and w_m are the weight of carbon fiber and matrix. ρ_{cf} and ρ_m are the density of carbon fiber and matrix. Table 4-2 shows the result.

Table 4-2 Volume fraction and recovery rate of samples

Lab length (mm)		12.5	25	50
Average recovery rate (%)	Hand-layup	43.1	70.3	79.8
	Printer	44.1	72	80.2
Standard deviation	Hand-layup	0.092	0.116	0.073
	Printer	0.052	0.060	0.022
Volume fraction (%)	Hand-layup	58.81		
	Printer	59.17		

$$* \text{ Recovery rate} = 100 \times \frac{\text{Repaired farcture load}}{\text{Undamaged fracture load}} \ (\%)$$

When the base laminate fabricates, the rigid mold and high pressure of post-curing make high fiber volume fraction. However, in the repair process, the different shape of the vacuum bag and pressure condition during the repair process makes different value of volume fraction. This could be caused by a difference between the volume of void for repairing process, voids are one of the most common manufacturing defects during the repair process. Void causes low stiffness of repair patches and resistance to contamination penetration. Voidage can be estimated via image-processing of cross-sections [8]. To check and compare the ratio of voidage, cross-sectional images are post-processed using the image-processing tool Image J to highlight void areas and compute ratios between the original and void areas. The detail of image-processing is achieved by the choice of detecting the fiber locations and radii on images using a Hough Transform. This method is known to be relatively unaffected by image noise [6]. Determining the radii range of fibers, it is possible to detect the individual fiber on the binary image. Finally, reconstructed clean the voidage image is achieved by reversing the image detected. The printer-repaired samples have void area approximately 0.6% of the cross-sections, while the corresponding figure for the hand-lay-up-repaired samples is 2.7%. The voidages and layer boundaries in the latter samples are mainly attributable to the binder used to maintain the fabric unidirectional. For the printer-repaired sample, the application of constant pressure during fiber printing and the use of non-bound dry fibers rendered uniform cross-sections possible.

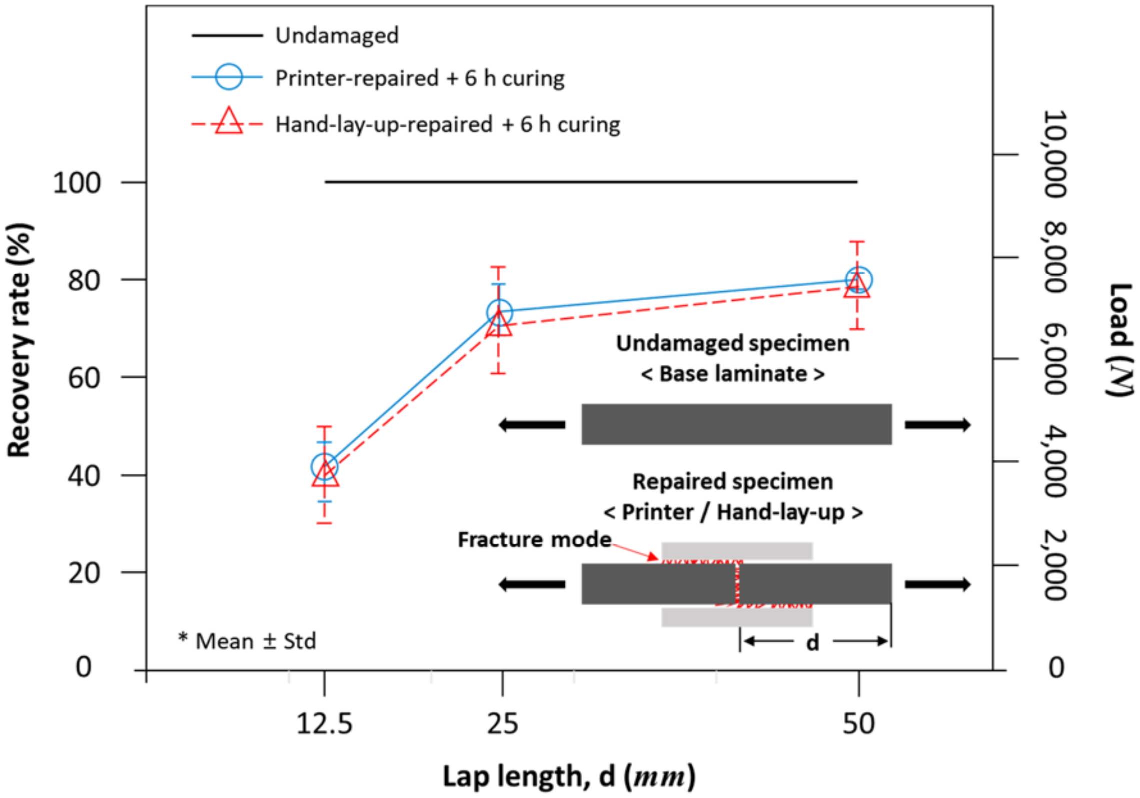

Figure 31 Recovery rate result between printer-repaired and hand lay-up-repaired specimens

4.2 Evaluation of degree of curing via rapid curing

Detail data for the tensile test between each different condition can check in Table 4-3. Except 130℃ and 30-min sample, the values of modulus are similar which means the property could be guaranteed. However, in the second graph means 90° sample from 100℃ and 5-min sample show lower modulus. It shows the amount of resin is an important issue for curing. These resin and hardener combinations can make the 0° sample which has around 130 GPa young's modulus and 1,300 MPa strength at fracture. 90° sample has around 10 GPa modulus and 40 MPa strength at fracture. This figure is enough for part of aero vehicle or car so if the amount of resin could be controlled, this parameter value is used on a rapid curing system. Based on this study, the proper condition for temperature and time with the proper amount of resin are determined. When 20 g of combination, the time for curing is reduced to around ten minutes. Using these parameters, the heating system will be discussed in the next chapter.

Table 4-3 Property test of CFRP according temperature vs. time

	Young's modulus (*GPa*)		Tensile strength (*MPa*)	
Test method	ASTM D 3039			
Degree of laminate (°) Cure condition (temp./time)	0	90	0	90
80℃ / 6 *h*	132.5	10.9	1,312	38.9
80℃ / 1 *h*	131.1	10.9	1,306	38.9
100℃ / 1 *h*	130.9	10.7	1,284	36.3
100℃ / 30 *m*	131.1	10.1	1,323	38.1
100℃ / 5 *m*	131.9	10.7	1,283	29.1
130℃ / 30 *m*	130.7	2.8	919	17.5

After this preliminary study about temperature versus time, the cross-sectional view of carbon fiber composite has been investigated qualitatively. Based on these pictures, image processing can measure the pore and the volume fraction of the composite. The comparison between the hand-lay-up repaired patch and printed repair patch is shown in Figure 32.

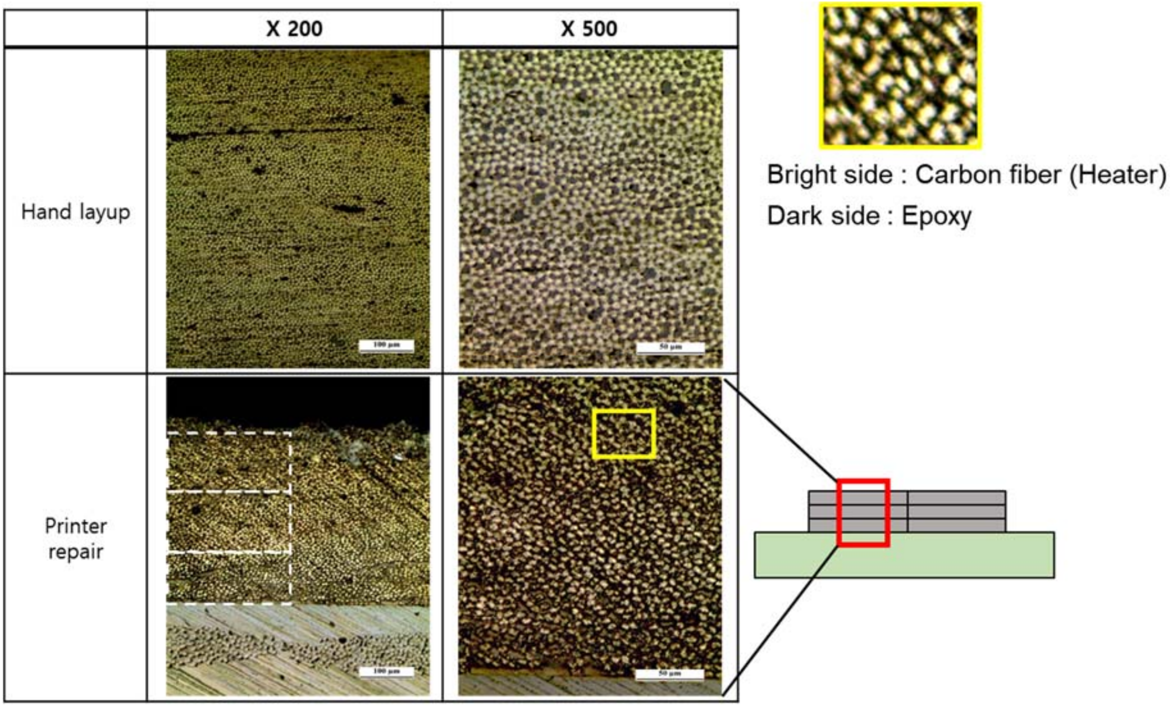

Figure 32 Comparison cross-section between hand-lay-up and printer-repair

As in Figure 32, bigger cracks hand-lay-up-repaired composite patch has bigger crack between the layers because this type of repair can load non-uniform pressure. According to this, verified the printer-repair makes parameter for repairing uniform.

For quantitative assessment study, measured data from dielectric cure monitoring (DEA) correlated with glass transition temperatures (T_g) are obtained from differential scanning calorimetry (DSC). Briefly defines this device, this application presents and discusses data for log (ion viscosity), which indicates the state of cure. For brevity, log will be called log (IV). Electrical conductivity (σ) has both frequency independent (σ_{DC}) and frequency dependent (σ_{AC}) components. In an oscillating electric field, σ_{DC} arises from the flow of mobile ions while σ_{AC} arises from the rotation of stationary dipoles. These two responses act in electrical elements in parallel and are added together as expressed below:

$$\sigma = \sigma_{DC} \sigma_{AC} \qquad (\mathrm{Ohm}^{-1} - \mathrm{cm}^{-1}) \tag{4-2}$$

Resistivity (ρ) is the inverse of conductivity and is defined as:

$$\rho = \frac{1}{\sigma} \qquad (\mathrm{Ohm} - \mathrm{cm}) \tag{4-3}$$

From its relationship to conductivity, resistivity also has both frequency-independent (ρ_{DC}) and frequency dependent (ρ_{AC}) components. Crosslink density, which is a measure of cure state, affects both mechanical viscosity and the movement of ions, and therefore influences ρ_{DC}. As a result, the term ion viscosity is coined to emphasize the relationship between mechanical viscosity and ρ_{DC}. Ion viscosity (IV) is defined as:

$$\mathrm{IV} = \rho_{DC} \quad (\mathrm{Ohm - cm}) \qquad (4\text{-}4)$$

It is hard to measure IV of actual sample so, the assumption for the test is shown in Figure 33. Insulation plate for resistance eruption used as a substrate. After that sensor with a thermocouple is mounted under the carbon fiber with epoxy. The electrical input condition which already found from the experiment case on carbon fiber with epoxy. The targeted pressure is also calculated and applied to the fiber structure.

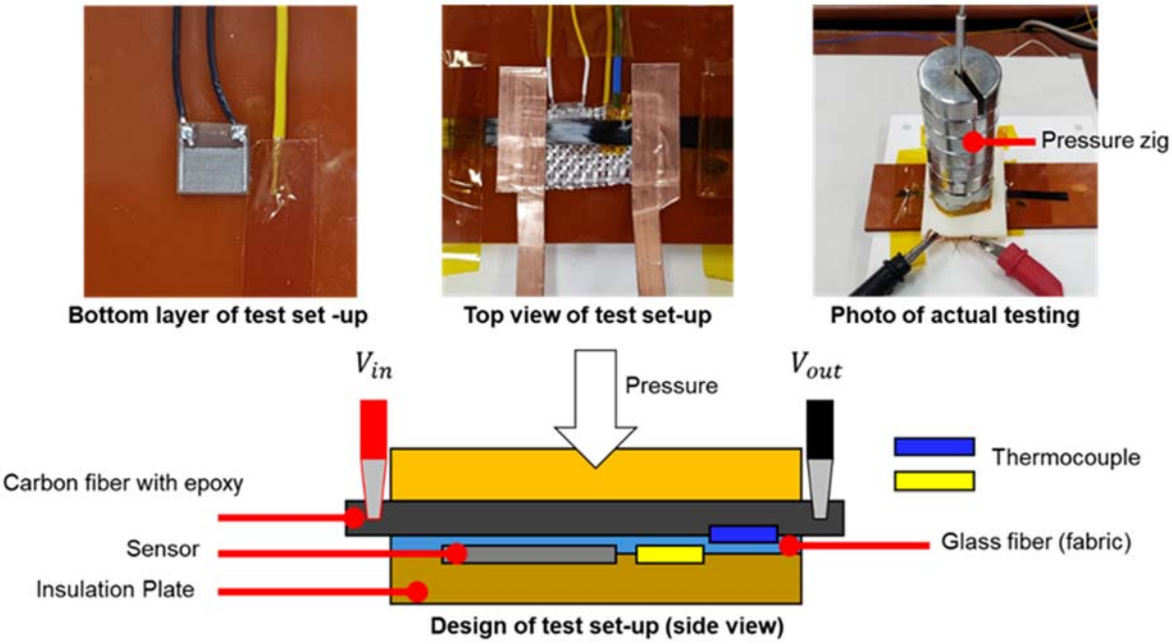

Figure 33 Test set up and configuration

Based on this experimental setup IV is mapped to the resistance value to obtain the result value over time. There are sometimes lags due to the characteristic of the experimental set-up, but even considering this, the clear time of the entire stream took place within a few minutes from the time when the temperature is raised, and this is a suitable condition for printing and processing simultaneously.

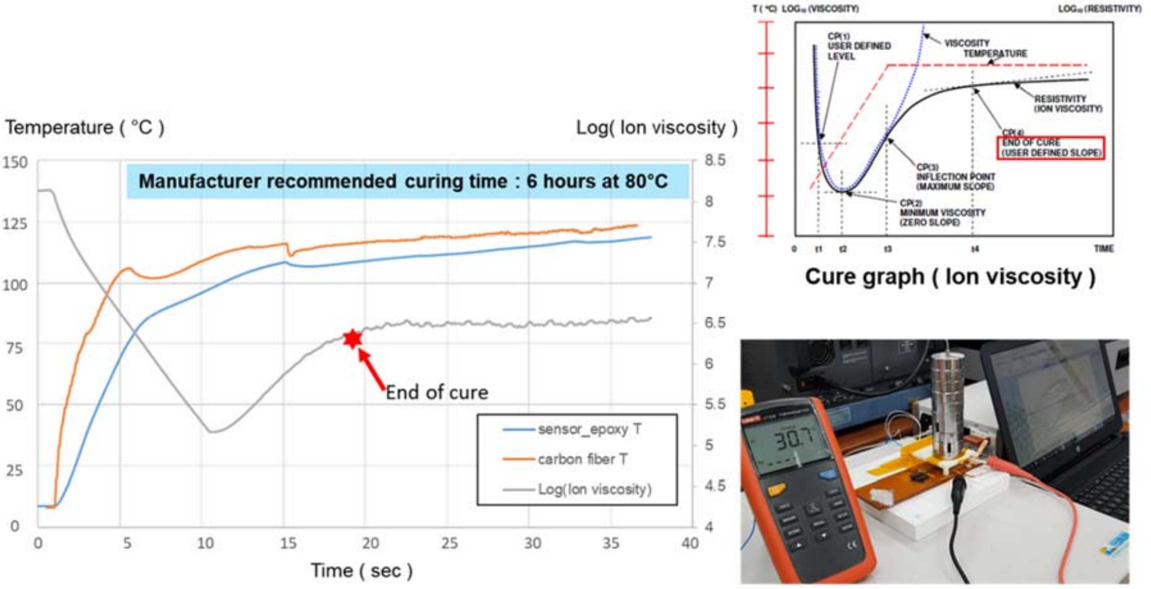

12W applied to the sample

Cure graph (Ion viscosity)

Actual time-temperature of carbon fiber

Figure 34 Test result of degree of cure

These two types of data, qualitative and quantitative data, could probe the sample fabricated using the rapid curing carbon fiber composite printer is able to achieve a high recovery rate compared with the reference sample. Figure 35 shows the result of proposed printer-repaired sample achieved 93% or higher recovery rate according to repair lap length.

From these data, the proposed system for repair patch printing is valuable to the public repair process which is not for skillful users. This machine can make some reference parameters for public users to repair their CFRP applications.

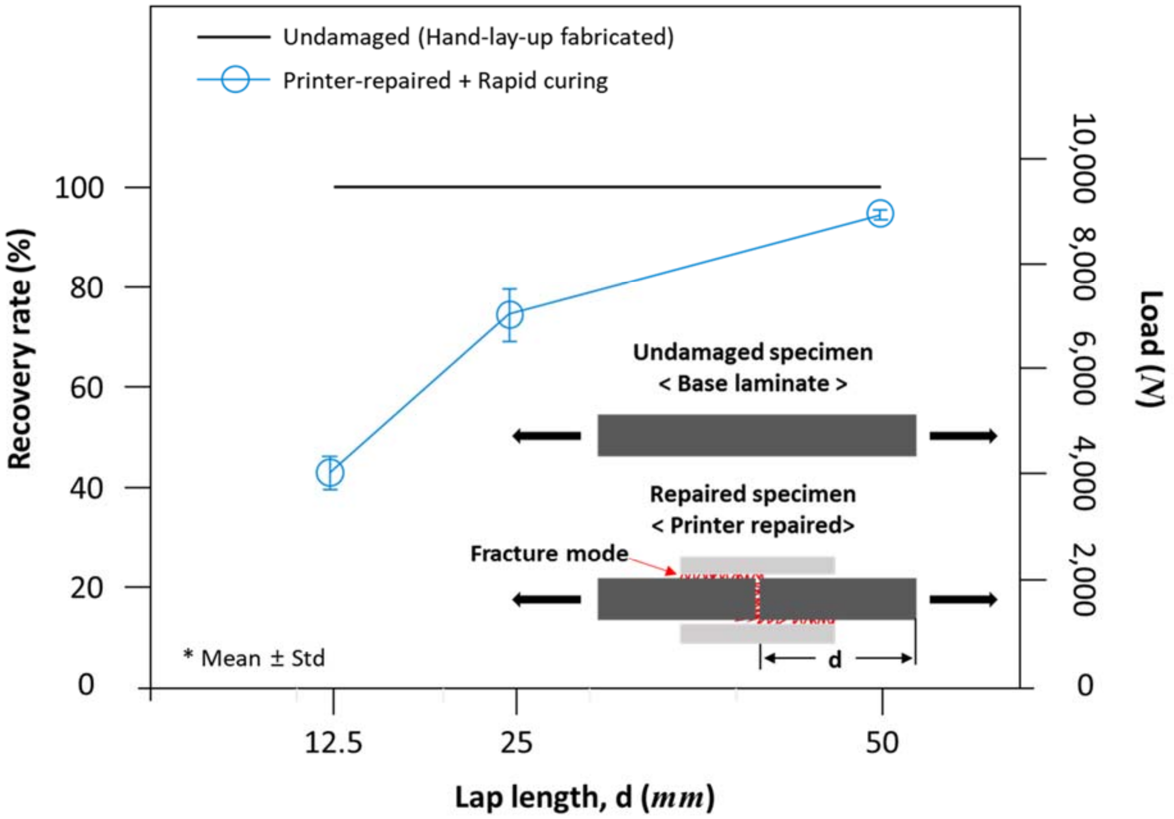

Figure 35 Recovery rate result of printer

with rapid curing system repaired specimens

4.3 Evaluation of SHM via communication system

To evaluate the sensor performance, an in-situ mechanical and electrical setup is constructed to measure the sensitivity and stretchability simultaneously. The printed sensor is stretched using the multi-axis stage (SGSP20, Sigma Koki, Japan) and relative resistance change is measured by LabVIEW 2015 and DAQ module (NI-6009, National Instruments, USA). Figure 36 shows the primary performance of the printed strain sensor. The maximum strain limit of this strain sensor can reach up to 74%. Besides, it possesses gauge factor of 58.7 in the same condition.

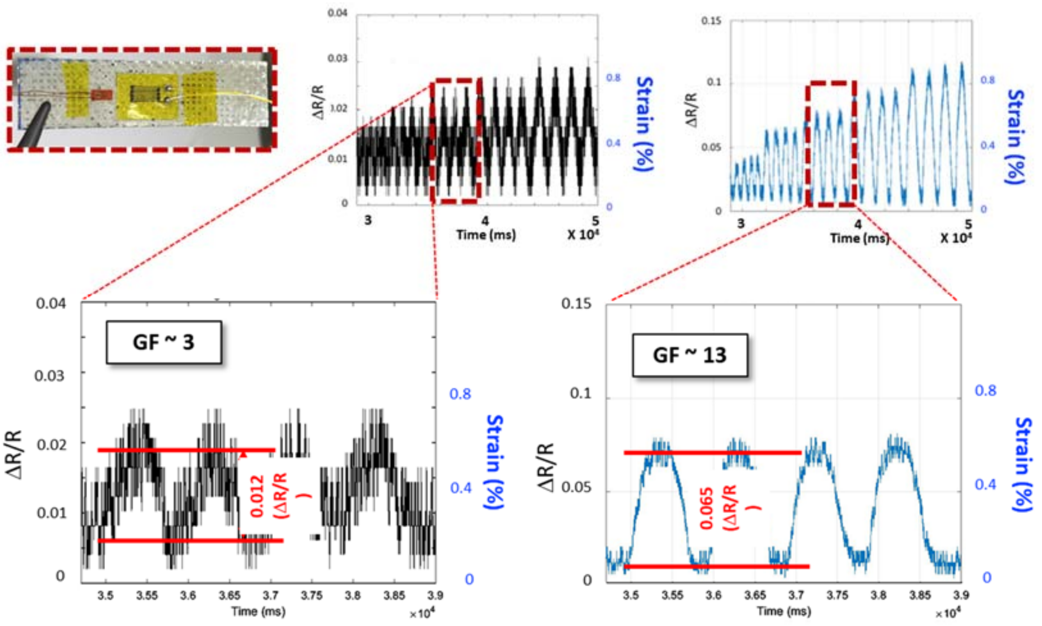

Figure 36 Comparison between commercial strain and printed sensor

In terms of scan time, it is verified that more scan time means a higher packing ratio for nanocomposites in the conductive line. Since the close distance between AgNPs prevents them from falling apart, a high packing ratio decreases the sensitivity of nanocomposites patterns [22, 72]. In this study, the scan time of about 20 s is the minimum value of strain sensor printing, which means that sensor printed with a scan time of at least 20 s is electrically connected. Hence, the gauge factor decreases as scan time increases due to the change of packing ratio.

Figure 36 shows sensitivity (gauge factor) for printed nanocomposites sensors. Metal NPs based sensors show high sensitivity, but low stretchability due to their sensing mechanism. The mechanical separation between NPs enables a drastic change of relative resistance, but also electrically disconnected above a specific level of strain. However, this characteristic of the proposed NP strain sensor is very proper for measuring microstrain of CFRP materials.

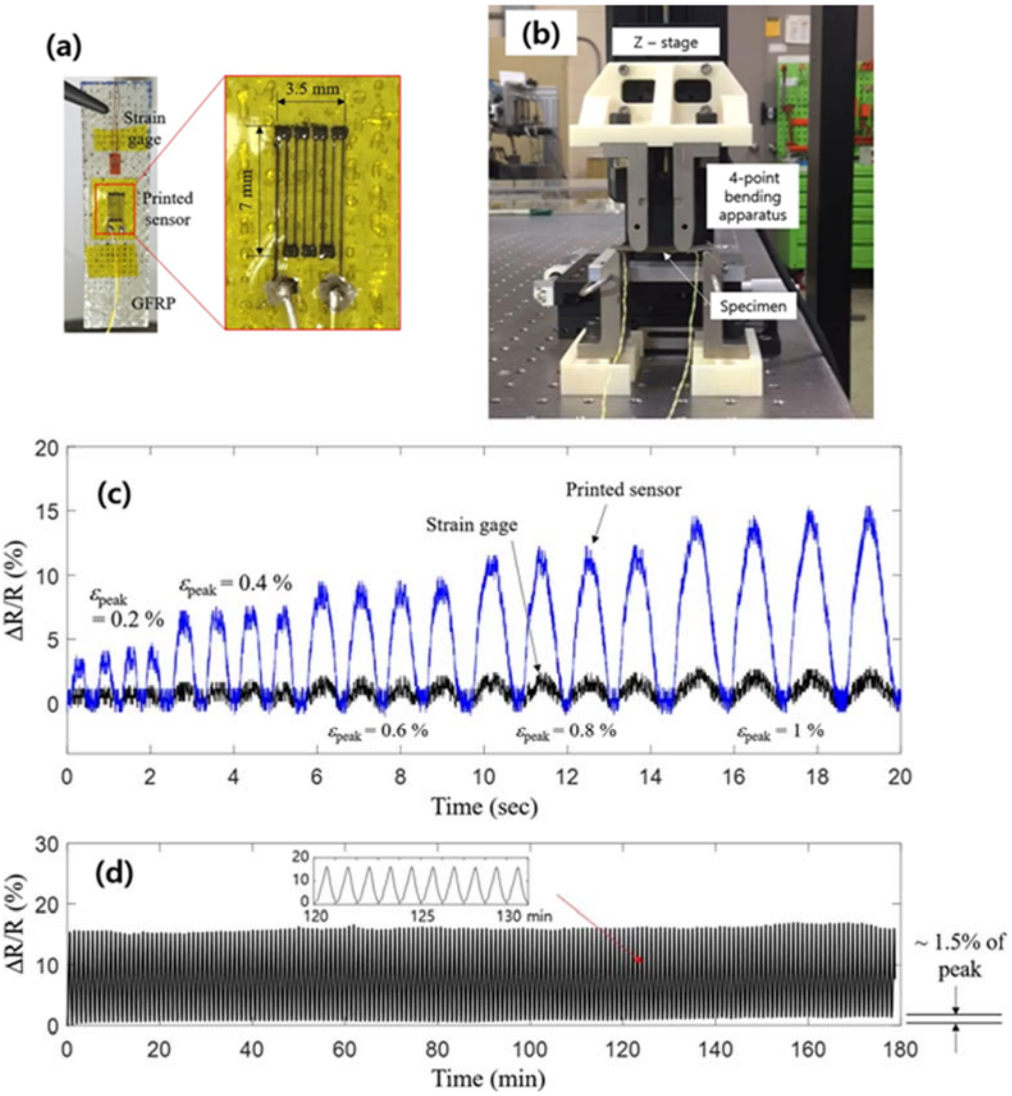

Figure 37 Life cycle test of the printed strain sensor

General conditions for SHM include airworthiness, cost-effectiveness, defect detection capability, and durability. Among these, the fabrication boundaries and conditions show this sensor can achieve airworthiness. Also, the characteristics of the proposed AgNP sensor are cheap price and simple manufacturing process. These achieve one of the general conditions for SHM, which is cost-efficiency.

Not just constraint conditions but performance conditions which are defect detection capability and durability are evaluated in Figure 36. Comparison between commercial strain and printed sensor is shown in Figure 37, life cycle test of the printed strain sensor. In the comparison gauge factor of the AgNP strain sensor shows more sensitive data measurement for CFRP materials and Figure 37 shows the bending test which also is produced and evaluated specimens referred to modified ASTM standard. This test was conducted over 3 hours with over 20,000 bending tests to identify the data values that are stable to use as SHM sensor measuring for the behavior of CFRP.

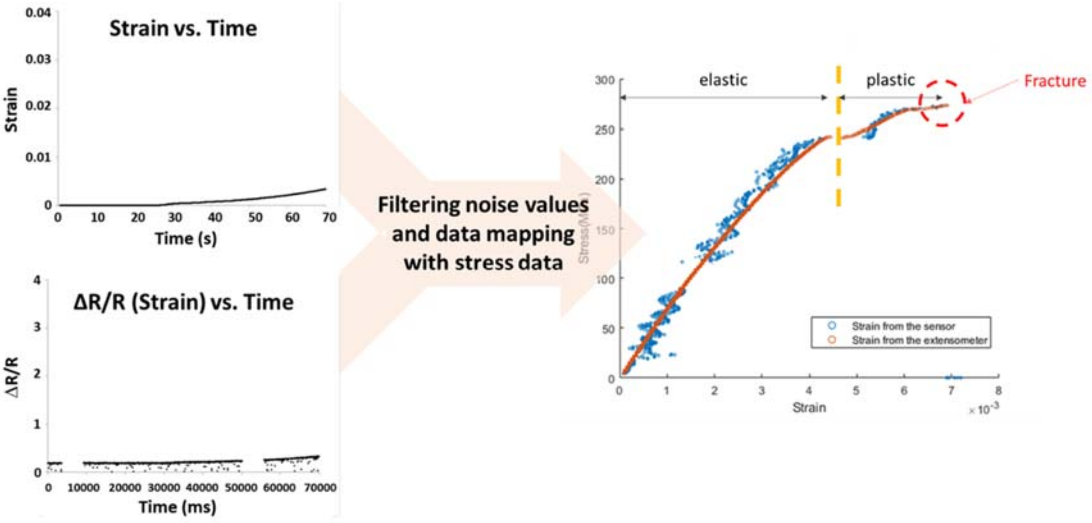

Figure 38 Comparison result between tethered vs. untethered data

After the evaluation of the AgNP strain sensor as the SHM sensor, the developed communication system is evaluated. Figure 38 shows the result of received data through the developed communication module mentioned in the previous chapter. The result presents there are able to make some noise and communication errors between the sender and receiver. However, this could be overcome by changing to the high-resolution component. Even though in this resolution, it is enough for observing and gathering the data for the behaviors of CFRP materials which are elastic, plastic region and fracture.

Chapter 5. Conclusion

In this dissertation, an approach to the manufacture of a composite printer for carbon/epoxy repair with a rapid curing system is presented. Three main points are expounded. First, an automated tape-laying system is proposed and designed. The research target is a repair patch for an aerospace component. Hence, the proper sizes of the roller and carbon fiber material are investigated and selected. The epoxy feeding parameter is investigated to identify an appropriate impregnation rate for continuous printing. The second key point is the rapid curing system. The electronic properties of carbon fiber suggest a novel approach to rapid curing based on Joule heating, which uses carbon fiber as the heating element. This type of heating was evaluated based on numerical analysis. According to our experimental results, the printed carbon-fiber composite, which was used as a bonded patch, exhibited a bond strength very similar to, or stronger than, that of the corresponding oven-cured hand-lay-up sample. Finally, a SHM module is also designed and fabricated for printed repair patches. To measure microstrain, we need to attach highly sensitive sensors to the repair patches. Hence, nanoparticle sensors were selected and their geometries were designed using the AFN printing system. A polyimide film was used to attach the sensor to the composite patch, and a simple wireless communication system was fabricated.

After fabricating the composite printing system, we compared the bond strengths of hand-lay-up and printed repaired samples. Using a printer, the parameters used to evaluate the repair process are standardized, the time taken to cut the patch to size is reduced, and the repeatability of the procedure is improved

A combination of epoxy and hardener for rapid curing was also investigated. Based on the results of our numerical analysis, we derived a formula to optimize the length of carbon fiber used for the heating element. A feedback module was also developed, as feedback between the thermal and electrical input signals can be used to generate uniform heat for epoxy-impregnated fiber. The degree of curing was also investigated and evaluated using the conventional discrete element analysis (DEA) method.

Finally, we discuss future work in which a robot will be mounted on the rapid curing carbon-fiber composite printing system. Automated mobile robots will also be used. Hence, the system proposed in this study is expected to help satisfy the increasing demand for various carbon-fiber composites and improve the processes for repairing carbon fiber components.

Bibliography

1. Ricci, F., Franco, F., & Montefusco, N. (2011). Bonded composite patch repairs on cracked aluminum plates: theory, modeling and experiments. Advances in Composite Materials-Ecodesign and Analysis, 445-464.
2. Baker, A. A., Rose, L. F., & Jones, R. (Eds.). (2003). Advances in the bonded composite repair of metallic aircraft structure. Elsevier.
3. Mahdi, S., Kim, H. J., Gama, B. A., Yarlagadda, S., & Gillespie Jr, J. W. (2003). A comparison of oven-cured and induction-cured adhesively bonded composite joints. Journal of composite materials, 37(6), 519-542.
4. Cheuk, P. T., Tong, L., Wang, C. H., Baker, A., & Chalkley, P. (2002). Fatigue crack growth in adhesively bonded composite-metal double-lap joints. Composite Structures, 57(1-4), 109-115.
5. Das, S. (2001). The cost of automotive polymer composites: a review and assessment of DOE's lightweight materials composites research (p. 47). Oak Ridge, Tennessee, USA: Oak Ridge National Laboratory.
6. Trias, D., Garc□a, R., Costa, J., Blanco, N., & Hurtado, J. E. (2007). Quality control of CFRP by means of digital image processing and statistical point pattern analysis. Composites Science and Technology, 67(11-12), 2438-2446.
7. Boudelier, A., Ritou, M., Garnier, S., & Furet, B. (2011). Optimization of process parameters in CFRP machining with diamond abrasive cutters. In Advanced Materials Research (Vol. 223, pp. 774-783). Trans Tech Publications.
8. Balakrishnan, V. S., Seidlitz, H., Ambrosio, M., & Schuhmann, T. (2017). Study on the quality of quasi-isotropic composite laminates containing a circular hole. J Mater Sci Res, 6(4), 67.
9. Usamentiaga, R., Venegas, P., Guerediaga, J., Vega, L., & L□pez, I. (2013). Automatic detection of impact damage in carbon fiber composites using active thermography. Infrared Physics & Technology, 58, 36-46.

10. Dirk, H. J. L., Potter, K. D., & Eales, J. (2013). A concept for the in situ consolidation of thermoset matrix prepreg during automated lay-up. Composites Part B: Engineering, 45(1), 538-543.
11. Sohn, H., Farrar, C. R., Hemez, F. M., Shunk, D. D., Stinemates, D. W., Nadler, B. R., & Czarnecki, J. J. (2003). A review of structural health monitoring literature: 1996–2001. Los Alamos National Laboratory, USA.
12. Lynch, J. P., & Loh, K. J. (2006). A summary review of wireless sensors and sensor networks for structural health monitoring. Shock and Vibration Digest, 38(2), 91-130.
13. Nagayama, T. and B.F. Spencer Jr, Structural health monitoring using smart sensors. 2007, Newmark Structural Engineering Laboratory. University of Illinois at Urbana.
14. Lee, J., Wu, F., Zhao, W., Ghaffari, M., Liao, L., & Siegel, D. (2014). Prognostics and health management design for rotary machinery systems—Reviews, methodology and applications. Mechanical systems and signal processing, 42(1-2), 314-334.
15. Culshaw, B. (2007). Health Monitoring of Aerospace Structures: Smart Sensor Technologies and Signal Processing Edited by W. Staszewski et al John Wiley and Sons, The Atrium, Southern Gate, Chichester, West Sussex, PO19 8SQ, UK, 2004. 266pp. Illustrated. $60. ISBN 0-470-84340-3. The Aeronautical Journal, 111(1125), 750-750.
16. Lynch, J. P., Farrar, C. R., & Michaels, J. E. (2016). Structural health monitoring: technological advances to practical implementations [scanning the issue]. Proceedings of the IEEE, 104(8), 1508-1512.
17. Abe, K., Suzuki, K., & Citterio, D. (2008). Inkjet-printed microfluidic multianalyte chemical sensing paper. Analytical chemistry, 80(18), 6928-6934.
18. Huang, L., Huang, Y., Liang, J., Wan, X., & Chen, Y. (2011). Graphene-based conducting inks for direct inkjet printing of flexible conductive patterns and their applications in electric circuits and chemical sensors. Nano Research, 4(7), 675-684.

19. Zhang, L., Liu, H., Zhao, Y., Sun, X., Wen, Y., Guo, Y., ... & Liu, Y. (2012). Inkjet printing high-resolution, large-area graphene patterns by coffee-ring lithography. Advanced Materials, 24(3), 436-440.

20. Pandita, S. D., Nishiyabu, K., & Verpoest, I. (2003). Strain concentrations in woven fabric composites with holes. Composite Structures, 59(3), 361-368.

21. Mahieux, C. A. (2005). Environmental degradation of industrial composites. Elsevier.

22. Tanner, J. L., Mousadakos, D., Giannakopoulos, K., Skotadis, E., & Tsoukalas, D. (2012). High strain sensitivity controlled by the surface density of platinum nanoparticles. Nanotechnology, 23(28), 285501.

23. Lee, G. Y., Park, J. I., Kim, C. S., Yoon, H. S., Yang, J., & Ahn, S. H. (2014). Aerodynamically focused nanoparticle (AFN) printing: novel direct printing technique of solvent-free and inorganic nanoparticles. ACS applied materials & interfaces, 6(19), 16466-16471.

24. Maier, A., Schmidt, R., Oswald-Tranta, B., & Schledjewski, R. (2014). Non-destructive thermography analysis of impact damage on large-scale CFRP automotive parts. Materials, 7(1), 413-429.

25. Lizaranzu, M., Lario, A., Chiminelli, A., & Amenabar, I. (2015). Non-destructive testing of composite materials by means of active thermography-based tools. Infrared Physics & Technology, 71, 113-120.

26. Ellert, F., Bradshaw, I., & Steinhilper, R. (2015). Major factors influencing tensile strength of repaired CFRP-samples. Procedia CIRP, 33, 275-280.

27. Schmidt, A. P. (2012). Faserverbundwerkstoffe im Automobilbau: methodischer Ansatz zur Analyse von Schäden.

28. Ahn, S. H., & Springer, G. S. (1998). Repair of composite laminates-I: test results. Journal of Composite Materials, 32(11), 1036-1074.

29. Baker, A. (2006). Development of a hard-patch approach for scarf repair of composite structure (No. DSTO-TR-1892). DEFENCE SCIENCE AND

TECHNOLOGY ORGANISATION VICTORIA (AUSTRALIA) AIR VEHICLES DIV.

30. Hart-Smith, L. J. (1973). Adhesive-bonded double-lap joints. NASA contract report.

31. Musto, P., Martuscelli, E., Ragosta, G., Russo, P., & Villano, P. (1999). Tetrafunctional epoxy resins: modeling the curing kinetics based on FTIR spectroscopy data. Journal of applied polymer science, 74(3), 532-540.

32. Wang, J., Rider, A. N., Heller, M., & Kaye, R. (2005). Theoretical and experimental research into optimal edge taper of bonded repair patches subject to fatigue loadings. International journal of adhesion and adhesives, 25(5), 410-426.

33. Kumar, A. M., & Hakeem, S. A. (2000). Optimum design of symmetric composite patch repair to centre cracked metallic sheet. Composite Structures, 49(3), 285-292.

34. Hailey, S. I., & Alden, J. W. (1987). U.S. Patent No. 4,707,212. Washington, DC: U.S. Patent and Trademark Office.

35. Olsen, H. B., & Craig, J. J. (1993, May). Automated composite tape lay-up using robotic devices. Proceedings IEEE International Conference on Robotics and Automation (pp. 291-297). IEEE.

36. Grimshaw, M. N., Grant, C. G., & Diaz, J. M. L. (2001, May). Advanced technology tape laying for affordable manufacturing of large composite structures. In International sampe symposium and exhibition (pp. 2484-2494). SAMPE; 1999.

37. Hauber, D. E., Langone, R. J., Martin, J. P., Miller, S. F., & Pasanen, M. J. (2006). U.S. Patent No. 7,063,118. Washington, DC: U.S. Patent and Trademark Office.

38. Martin, J. P. (2007). U.S. Patent No. 7,293,590. Washington, DC: U.S. Patent and Trademark Office.

39. Farrar, C. R., & Lieven, N. A. (2006). Damage prognosis: the future of structural health monitoring. Philosophical Transactions of the Royal

Society A: Mathematical, Physical and Engineering Sciences, 365(1851), 623-632.

40. Brajou, F., & Ricco, P. (2004, September). The Airbus A380-an AFDX-based flight test computer concept. In Proceedings AUTOTESTCON 2004. (pp. 460-463). IEEE.

41. Norris, G., & Wagner, M. (2005). Airbus A380: superjumbo of the 21st century. Zenith Imprint.

42. Forsyth, P. (2005). Airport infrastructure for the Airbus A380: cost recovery and pricing. Journal of Transport Economics and Policy (JTEP), 39(3), 341-362.

43. Ramsey, J. W. (2005). Boeing 787: Integration's Next Step. Avionics Magazine, 29(6), 20.

44. Whinnem, E., Lipczynski, G., & Eriksson, I. (2008). Development of orbital drilling for the Boeing 787. SAE International Journal of Aerospace, 1(2008-01-2317), 811-816.

45. Wagner, M., & Norris, G. (2009). Boeing 787 dreamliner. Zenith Press.

46. Denning, S. (2013). What went wrong at Boeing. Strategy & Leadership, 41(3), 36-41.

47. Rose, L. R. F. (1981). An application of the inclusion analogy for bonded reinforcements. International Journal of Solids and Structures, 17(8), 827-838.

48. Baker, A. A., Callinan, R. J., Davis, M. J., Jones, R., & Williams, J. G. (1984). Repair of Mirage III aircraft using the BFRP crack-patching technique. Theoretical and Applied Fracture Mechanics, 2(1), 1-15.

49. Naboulsi, S., & Mall, S. (1996). Modeling of a cracked metallic structure with bonded composite patch using the three layer technique. Composite Structures, 35(3), 295-308.

50. Schubbe, J. J., & Mall, S. (1999). Investigation of a cracked thick aluminum panel repaired with a bonded composite patch. Engineering Fracture Mechanics, 63(3), 305-323.

51. Klug, J., Maley, S., & Sun, C. T. (1999). Characterization of fatigue behavior of bonded composite repairs. Journal of aircraft, 36(6), 1016-1022.

52. Naboulsi, S., & Mall, S. (1998). Nonlinear analysis of bonded composite patch repair of cracked aluminum panels. Composite Structures, 41(3-4), 303-313.

53. Chung, K. H., & Yang, W. H. (2002). Fracture mechanics analysis on the bonded repair of a skin/stiffener with an inclined central crack. Composite Structures, 55(3), 269-276.

54. Feraboli, P., Peitso, E., Deleo, F., Cleveland, T., & Stickler, P. B. (2009). Characterization of prepreg-based discontinuous carbon fiber/epoxy systems. Journal of reinforced plastics and composites, 28(10), 1191-1214.

55. Tsuchiya, A., Honma, M., Sasaki, H., & Murai, S. (2011). U.S. Patent No. 8,071,205. Washington, DC: U.S. Patent and Trademark Office.

56. Dirk, H. J. L., Ward, C., & Potter, K. D. (2012). The engineering aspects of automated prepreg layup: History, present and future. Composites Part B: Engineering, 43(3), 997-1009.

57. Uchida, T., Hamada, H., Kuroda, K., Endo, A., Migaki, M., Ochiai, J., ... & Goto, A. (2015, August). Process analysis of the hand lay-up method using CFRP prepreg sheets. In International Conference on Digital Human Modeling and Applications in Health, Safety, Ergonomics and Risk Management (pp. 227-236). Springer, Cham.

58. Campilho, R. D. S. G., De Moura, M. F. S. F., Pinto, A. M. G., Morais, J. J. L., & Domingues, J. J. M. S. (2009). Modelling the tensile fracture behaviour of CFRP scarf repairs. Composites Part B: Engineering, 40(2), 149-157.

59. Wang, C. R., Gu, Y. Z., Zhang, K. M., Li, M., & Zhang, Z. G. (2013). Rapid curing epoxy resin and its application in carbon fibre composite fabricated using VARTM moulding. Polymers and Polymer Composites, 21(5), 315-324.

60. Hu, X., Ravikumar, D., & Patten, D. (2014). U.S. Patent Application No. 14/295,402.

61. Rudnev, V., Loveless, D., & Cook, R. L. (2017). Handbook of induction heating. CRC press.

62. Barrag□n, L. A., Navarro, D., Acero, J., Urriza, I., & Burd□o, J. M. (2008). FPGA implementation of a switching frequency modulation circuit for EMI reduction in resonant inverters for induction heating appliances. IEEE Transactions on Industrial Electronics, 55(1), 11-20.

63. Jungwirth, M., & Hofinger, D. (2007). Multiphysics modelling of high-frequency inductive devices. In The Proceeding of the COMSOL Users conference.

64. Oesterle, L. J., Newman, S. M., & Shellhart, W. C. (2001). Rapid curing of bonding composite with a xenon plasma arc light. American Journal of Orthodontics and Dentofacial Orthopedics, 119(6), 610-616.

65. Odom, M. G., Sweeney, C. B., Parviz, D., Sill, L. P., Saed, M. A., & Green, M. J. (2017). Rapid curing and additive manufacturing of thermoset systems using scanning microwave heating of carbon nanotube/epoxy composites. Carbon, 120, 447-453.

66. Bogetti, T. A., & Gillespie Jr, J. W. (1991). Two-dimensional cure simulation of thick thermosetting composites. Journal of composite materials, 25(3), 239-273.

67. Guo, Z. S., Du, S., & Zhang, B. (2005). Temperature field of thick thermoset composite laminates during cure process. Composites science and technology, 65(3-4), 517-523.

68. Mas, B., Fernndez-Blzquez, J. P., Duval, J., Bunyan, H., & Vilatela, J. J. (2013). Thermoset curing through Joule heating of nanocarbons for composite manufacture, repair and soldering. Carbon, 63, 523-529.

69. Sung, P. C., & Chang, S. C. (2015). The adhesive bonding with buckypaper–carbon nanotube/epoxy composite adhesives cured by Joule heating. Carbon, 91, 215-223.

70. Gil-yong Lee, (2013). Multi-material Direct Printing by Pulsed-Nano Particle Deposition System (P-NPDS) (Doctoral dissertation, Seoul National University).

71. Jones, R. M. (2014). Mechanics of composite materials. CRC press.

72. Chen, S., Wei, Y., Yuan, X., Lin, Y., & Liu, L. (2016). A highly stretchable strain sensor based on a graphene/silver nanoparticle synergic conductive network and a sandwich structure. Journal of Materials Chemistry C, 4(19), 4304-4311.

요약 (국문초록)

탄소 에폭시 수리를 위한 복합재 프린터

김호진

서울대학교 일반대학원

기계항공공학부 기계공학전공

탄소 섬유 복합재의 수요는 비행기 산업 및 풍력 발전 산업 등에서 많이 사용되어 왔으며, 전기차의 발전으로 인해 경량소재에 대한 관심 또한 증가하면서 더욱 많은 수요가 발생하였다. 이에 따라 이 제품들을 사용하는 사용자들의 수리 방법에 대한 연구가 진행되어왔으며, 섬유 복합재의 특성상 수리된 부위의 파괴 수준을 측정하기 어렵고, 이를 확인한 후에도 수리과정이 작업자의 손을 이용한 작업이 주된 방법이다. 이 방법은 수리자의 숙련도에 크게 수리의 성능이 좌우되는 방법이며, 수리부위의 크기와 형태에 따라 탄소 섬유를 재단하는데 큰 노동과 시간이 들어간다. 또한 복합재의 다른 특성인 후경화 과정은 수리과정에서 긴 시간을 요구하며, 이는 수리 부위의 크기와 상관없이 긴 시간이 걸리기 때문에 자동차 부분 파손 혹은 휴대폰 외관 수리와 같은 작은 파트를 수리하는 부분에 있어 큰 낭비가 될 수 있다. 수리를 완료한 이후에도 이 수리부의 수명이나 변형을 측정함으로써, 사용자가 파손을 예측하고 대비하고 정도에 따라 수리과정을 준비할 방법 또한 필요하다.

본 연구에서는 위와 같은 문제들에 대하여 사람의 손으로 진행해야 하는 부분을 자동화함으로써 변수를 통합 및 안정화하고, 긴 시간을 차지하는 후경화를 국지적 주울열을 통한 급속 경화 장치를 추가함으로써 급속 경화 탄소 섬유 복합재 프린터를 개발하였다. 기존의 비행기나 대형 탄소복합재를 만들기 위한 Automated tape laying (ATL) 과 같은 대형 장비들에 대한 연구들이 2016 부터 활발히 진행되었으나, 기존 연구의 대부분은 대형 탄소 섬유 복합재를

제작하는 것을 목적으로 진행하고 있어, 후경화의 단축에 대한 연구수행과 소규모성의 수리를 위한 자동화 공정에 대한 연구는 여전히 부족한 실정이다. 또한 본 연구의 국지적 수리에 적합한 주울열을 통한 급속 경화 장치가 적용된 사례는 없다.

이와 같이 본 연구에서 제안된 프린팅 시스템을 이용하여 양면 접착 방식의 수리 시편을 만들어 기존 미파괴 시편과의 파단강도에 따른 비율을 회복률이라고 정의하였다. 또한 실험을 통해 회복률을 확인하였고, 프린팅을 통한 수리 시편은 인장강도 기준으로 80% 이상 수준을 달성하였고 급속 경화 시스템을 추가한 시편의 경우는 짧은 구간에서 더 높은 접착력을 보이면서 93%이상 회복률로 향상되었다. 또한 앞서 제시한 바와 같이 수리자의 숙련도에 따라 변경될 수 있는 수리 성능에 대한 변수를 규격화 하였으며, 온도와 전력량 간의 피드백 시스템을 형성하여 급속 경화 또한 최적화함으로써 사용자의 숙련도와 상관없이 균일한 회복률을 얻을 수 있는 효과를 얻었고 이에 접착 수리 패치의 수명과 대변형과 같은 수리파손 예방을 위한 나노입자 센서를 부착하고 무선통신 시스템을 적용함으로써 비파괴 검사 또한 진행할 수 있도록 하였다. 본 연구에서 제안된 급속 경화 탄소 복합재 프린터와 이를 검사할 수 있는 시스템의 원리를 응용한 기술은 발전될 탄소 섬유를 이용한 전기차 혹은 휴대기기 시장 등 산업적 응용 분야 확장에 기여할 것으로 기대된다.

중심어: 탄소 복합재, 삼차원 프린터, 주울열 가열, 급속 경화, 구조 안전 모니터링, 자동화 공정

학번: 2014-21832